ISTANBUL TECHNICAL UNIVERSITY ★ GRADUATE SCHOOL

ESTIMATED POSITION ERROR REDUCTION OF SMO-BASED SENSORLESS CONTROL OF IPMSM USING VARIABLE NOTCH FILTER

M.Sc. THESIS

Navid DELFEKAR BAGHBANI

Department of Electrical Engineering

Electrical Engineering Programme

JUNE 2023

ISTANBUL TECHNICAL UNIVERSITY ★ GRADUATE SCHOOL

ESTIMATED POSITION ERROR REDUCTION OF SMO-BASED SENSORLESS CONTROL OF IPMSM USING VARIABLE NOTCH FILTER

M.Sc. THESIS

Navid DELFEKAR BAGHBANI
(504191086)

Department of Electrical Engineering

Electrical Engineering Programme

Thesis Advisor: Assoc. Prof. Dr. Salih Barış ÖZTÜRK

JUNE 2023

İSTANBUL TEKNİK ÜNİVERSİTESİ ★ LİSANSÜSTÜ EĞİTİM ENSTİTÜSÜ

NOTCH FİLTRE KULLANARAK IPMSM'İN KAYAN KİPLİ SENSÖRSÜZ KONTROLÜNDE KONUM HATASININ AZALTILMASI

YÜKSEK LİSANS TEZİ

Navid DELFEKAR BAGHBANI
(504191086)

Elektrik Mühendisliği Anabilim Dalı

Elektrik Mühendisliği Programı

Tez Danışmanı: Doç. Dr. Salih Barış ÖZTÜRK

HAZİRAN 2023

Navid DELFEKAR BAGHBANI, a M.Sc. student of ITU Graduate School student ID 504191086, successfully defended the thesis entitled "ESTIMATED POSITION ERROR REDUCTION OF SMO-BASED SENSORLESS CONTROL OF IPMSM USING VARIABLE NOTCH FILTER", which he prepared after fulfilling the requirements specified in the associated legislations, before the jury whose signatures are below.

Thesis Advisor :	**Assoc. Prof. Dr. Salih Barış ÖZTÜRK** Istanbul Technical University	.....
Jury Members :	**Assoc.Prof.Dr.Derya Ahmet KOCABAŞ** Istanbul Technical University	.....
	Assoc. Prof. Dr. Ömer Cihan KIVANÇ Okan University	.....

Date of Submission : 26 May 2023
Date of Defense : 19 June 2023

To my family,

FOREWORD

The base idea of this thesis is to reduce the position estimation error arising from oscillation by employing a variable notch filter in a sliding mode observer sensorless control which is simulated in Matlab. This thesis is done upon completion of a Master's degree at the Electrical Engineering Department, Istanbul Technical University (ITU).

I would like to express my special appreciation to my supervisor Assoc. Prof. Dr. Salih Barış Öztürk for his support and guidance throughout this thesis work.

Besides my supervisor, I would also like to thank Istanbul Technical University and Turkey for giving me the opportunity to start a new challenge in my life. I have learned a lot while accomplishing my journey here at ITU.

June 2023 Navid DELFEKAR BAGHBANI

TABLE OF CONTENTS

Page

ABBREVIATIONS

PMSM	**:**	Permanent Magnet Synchronous Motor
PWM	**:**	Pulse Width Modulation
RPM	**:**	Revolutions per Minute
SMO	**:**	Sliding Mode Observer
PI	**:**	Proportional-Integral
EMF	**:**	Electromagnetic Force
BEMF	**:**	Back Electromagnetic Force
IPMSM	**:**	Interior Permanent Magnet Synchronous Motor
LPF	**:**	Low-Pass Filter
PLL	**:**	Phase-Locked Loop

SYMBOLS

$i_{s(a,b,c)}$	: Stator Current in Three-phase Reference Frame
$i_{s(d,q)}$	: Stator Current in d-q Reference Frame
$i_{s(\alpha,\beta)}$	: Stator Current in $\alpha - \beta$ Reference Frame
ω_e	: Electrical Rotor Speed
R_s	: Stator Resistance
L_d	: Stator Inductance in d-axis
L_q	: Stator Inductance in q-axis
α-β	: Orthogonal Stationary Reference Frame
d-q	: Rotating Reference Frame
v_{as}	: Stator Voltage of phase a
v_{bs}	: Stator Voltage of phase b
v_{cs}	: Stator Voltage of phase c
i_{as}	: Stator Current of phase a
i_{bs}	: Stator Current of phase b
i_{cs}	: Stator Current of phase c
λ_m	: Permanent Magnet Flux
λ_{as}	: Stator Flux of phase a
λ_{bs}	: Stator Flux of phase b
λ_{cs}	: Stator Flux of phase c
λ_{ma}	: Permanent Magnet Flux of phase a
λ_{mb}	: Permanent Magnet Flux of phase b
λ_{mc}	: Permanent Magnet Flux of phase c
$L_{a,b,c}$	: Stator Inductance
L_{aa}	: Stator Self-inductance of phase a
L_{bb}	: Stator Self-inductance of phase b
L_{cc}	: Stator Self-inductance of phase c
L_{ab}	: Stator Mutual-inductance of phase a and b
L_{ba}	: Stator Mutual-inductance of phase a and b
L_{bc}	: Stator Mutual-inductance of phase b and c
L_{cb}	: Stator Mutual-inductance of phase b and c
L_{ac}	: Stator Mutual-inductance of phase a and c
L_{ca}	: Stator Mutual-inductance of phase a and c
L_{sr}	: Space Fundamental Self-inductance
L_{sl}	: Armature Leakage Inductance
L_{g2}	: Rotor Position-dependent Inductance

$\boldsymbol{\theta_r}$: Rotor Electric Angle
$\boldsymbol{\hat{e}_{s(\alpha,\beta)}}$: Estimated BEMF in $\alpha - \beta$ Reference Frame
$\boldsymbol{\hat{e}_{s(d,q)}}$: Estimated BEMF in d-q Reference Frame
$\boldsymbol{\hat{i}_{s(\alpha,\beta)}}$: Estimated Stator Currents in $\alpha - \beta$ Reference Frame
$\boldsymbol{\hat{i}_{s(d,q)}}$: Estimated Stator Currents in d-q Reference Frame
$\boldsymbol{e_{s(d,q)}}$: BEMF in d-q Reference Frame
$\boldsymbol{e_{\alpha,\beta}}$: BEMF in $\alpha - \beta$ Reference Frame
$\mathbf{g_1}$: SMO Feedback Gain
$\boldsymbol{\varepsilon_{1(\alpha,\beta)}}$: Current Estimation Error in $\alpha - \beta$ Reference Frame
$\boldsymbol{\varepsilon_{1(d,q)}}$: Current Estimation Error in d-q Reference Frame
$\boldsymbol{\varepsilon_{2(\alpha,\beta)}}$: BEMF Estimation Error in $\alpha - \beta$ Reference Frame
$\boldsymbol{\varepsilon_{2(d,q)}}$: BEMF Estimation Error in d-q Reference Frame
$\boldsymbol{\omega_n}$: Notch Frequency
$\boldsymbol{f_c}$: Input Frequency
$\boldsymbol{f_s}$: Sampling Frequency

LIST OF TABLES

Page

LIST OF FIGURES

Page

ESTIMATED POSITION ERROR REDUCTION OF SMO-BASED SENSORLESS CONTROL OF IPMSM USING VARIABLE NOTCH FILTER

SUMMARY

Controlling IPMSM is categorized into two sections; an open-loop strategy in which the essence of shaft position information is not needed and a close-loop strategy in which shaft's position information is required and is subdivided into two methods:

- Sensored
- Sensorless

In the sensorless method, there are three methods for rotor position estimation. The first one is fundamental excitation which includes adaptive and non-adaptive methods. Secondly, signal injection methods, and the last one is the help of artificial intelligence.

Adaptive methods are categorized as model reference adaptive base systems and observer-based control, which is subdivided into Luenberger Observer, reduced order observer, sliding mode observer (SMO), and Kalman filter.

Estimation error in SMO control is inevitable, and it is generated because of its sign function. In this work, a sliding mode observer is employed, and the error in this method is reduced by applying varying notch filters in the system. When a system's state is not measured directly, sliding mode observer control can be utilized to estimate the required dynamics. The main function of SMO is moving or sliding over a hyperplane to reach the desired or stable state and stays on it. With the help of these estimated state variables, it is possible to control our system. In the case of controlling IPMSM, the estimated state variables are the rotor's speed and position.

A sign function is employed to determine the hyperplane. By multiplying the sign function of estimated value minus real value, the sliding surface is defined. If the sliding surface converges to zero, the error between the estimated and real value approaches to zero. The sign function, which is the main part of SMO, creates oscillations in the system and causes chattering in IPMSM. In order to overcome this obstacle, filtering the oscillated frequency is proposed. The range of the frequency which is being eliminated from the output of SMO should be narrow so that a notch filter is suggested to attenuate the oscillation frequency. In this case, in which the parameters of IPMSM have already been defined, the oscillated frequency for reference speed of 0.1 pu is obtained from the FFT analysis of the signal, which is 27.34 Hz.

After simulating the proposed method in MATLAB®/Simulink® and filtering the aforementioned frequency from the estimated speed, a significant reduction in the first harmonic oscillation of the signal is achieved, and according to its FFT frequency

response, its amplitude is decreased from 0.14 to 0.05 when the motor is rotating at 0.1 pu.

In conclusion, this method has reduced chattering in the system and attenuated the frequency, which leads to estimation error mitigation, and increases the robustness and accuracy of the position sensing of IPMSM.

NOTCH FİLTRE KULLANARAK IPMSM'İN KAYAN KİPLİ SENSÖRSÜZ KONTROLÜNDE KONUM HATASININ AZALTILMASI

ÖZET

IPMSM'nin kontrolü iki bölüme ayrılmıştır; Şaft pozisyon bilgisinin gerekli olmadığı açık döngü stratejisi ve şaft pozisyon bilgisinin gerekli olduğu kapalı döngü stratejisi olarak ikiye ayrılır:

- Sensörlü
- Sensörsüz

Sensörsüz yöntemde, rotor konum tahmini için üç yöntem vardır. Bunlardan ilki adaptif ve adaptif olmayan yöntemleri içeren temel uyarımdır. İkincisi, sinyal enjeksiyon yöntemleri ve sonuncusu yapay zeka kullanımıdır.

Uyarlanabilir yöntemler, model referanslı uyarlanabilir temel sistemler ve Luenberger Gözlemcisi, azaltılmış dereceli gözlemci, kayan kipli gözlemci (SMO) ve Kalman filtresi olarak alt bölümlere ayrılan gözlemci tabanlı kontrol olarak kategorize edilir. Bu çalışmada kayan kipli gözlemci kullanılmıştır.

Harmonikler, doğrusal olmayan bir sistemin kaçınılmaz parametreleridir; IPMSM kontrolünde doğrusal olmama, ideal olmayan inverter, inverterde ölü zamanın varlığı, akı uzamsal bağlantısı ve parametre değişimleri tarafından üretilir. SMO sensörsüz kontrol durumunda, bu harmonikler kestirimi etkiler ve kestirilen hız ve konum rotor dönüş frekansına bağlı olarak dalgalanır. Sistemdeki hata oranını artıran bu dalgalanmayı azaltmak için değişken bir çentik (notch) filtresi önerilmektedir. Bu filtreyi kullanmak, dönüş frekansı ile ilişkili olan istenen harmoniği ortadan kaldırmamıza fayda sağlar.

Bir sistemin durumu doğrudan ölçülemediğinde, gerekli dinamikleri tahmin etmek için kayan kip gözlemci kontrolü kullanılabilir. SMO'nun ana işlevi, istenen veya kararlı duruma ulaşmak için bir hiper düzlem üzerinde hareket etmek veya kaymak ve bunun üzerinde kalmaktır. Gözlemcinin amacı, tahmin edilen durumları doğru bir şekilde belirlenebilecekleri bu kayan yüzeye sürmektir. Durumlar kayan yüzey üzerinde olduğunda, gözlemci bu tahmini durum bilgisine dayanarak kontrol sinyalleri üretebilir. Bu tahmini durum değişkenlerinin yardımıyla sistemimizi kontrol etmek mümkündür. IPMSM'nin kontrol edilmesi durumunda, tahmin edilen durum değişkenleri rotorun hızı ve konumudur.

Hiper düzlemi belirlemek için bir işaret fonksiyonu kullanılır. Kestirilen değer eksi gerçek değer işaret fonksiyonu ile çarpılarak kayan yüzey tanımlanır. Kayan yüzey sıfıra yakınsarsa tahmini ve gerçek değer arasındaki hata sıfıra yaklaşır. SMO'nun ana parçası olan işaret fonksiyonu sistemde salınımlar yaratır ve IPMSM'de gevezeliğe

neden olur. kayan mod gözlemci kontrolü, kontrol sistemlerinde durum tahmini için kullanılan bir tekniktir. Kayan bir yüzey ve tahmin edilen durumları kayan yüzeye sürmek için işaret fonksiyonunu kullanır ve belirsizliklerin ve bozulmaların varlığında bile doğru tahmin yapılmasını sağlar. İşaret fonksiyonu, kayan yüzeyi tanımlamak ve gözlemcinin dinamiklerini tasarlamak için kullanılır, bu da sağlam ve ayrık gözlemci yanıtları sağlar. Bu engelin üstesinden gelmek için salınan frekansın filtrelenmesi önerilmiştir. SMO'nun çıkışından elimine edilen frekans aralığı dar olmalıdır, bu nedenle salınım frekansını zayıflatmak için bir çentik filtresi önerilmektedir.

Filtreler, sistemdeki geri beslemeyi bozan gürültü ve istenmeyen rezonansları azaltarak kontrol sistemlerinde ana rol oynar. Çoğunlukla filtreler iletişim mühendisleri tarafından bozulmayı azaltmak için kullanılır, burada bu filtreleri kontrol mühendisliği perspektifinden geri besleme ve tahmindeki gereksiz sinyallerin etkisini azaltmak için kullanıyoruz. Filtrelerin ana dezavantajları, kazanç geçiş frekansı gibi belirli frekanslarda faz gecikmesi nedeniyle oluşan kararsızlıktır. Çentik filtreleri, tasarımları sayesinde, bu uygulamalarda daha az sınırlıdır, bu filtre için hem avantaj hem de dezavantaj diğer filtrelere göre daha az yoğundur. Bu tezde çentik filtresine genel bir bakış yapılmış ve bu filtrenin matematiksel denklemleri sunulmuş ve tartışılmıştır. Çentik filtre, iki sıfır ve iki kutuplu ikinci dereceden bir filtredir, kutuplar hafif sönümlüdür ve sıfır-kutup diyagramında gösterildiği gibi özelliğine göre kutuplar ve sıfırlar birbirine çok yakındır. Sönüm oranı, ζ, çentik filtresinde genellikle 1.0'ın altında ayarlanır, daha keskin bir filtre elde etmek için ζ daha düşük değerlere ayarlanmalıdır, dolayısıyla ζ ne kadar düşük olursa, o kadar keskin kazanç elde edilir. İstenen sinyali iyice zayıflatmak için, katsayıların hassas seçimi gereklidir. Yüksek ζ filtrenin merkezde daha fazla yoğunlaşmasına neden olur. "Değişken" terimi, çentiğin merkez frekansının, filtrenin katsayılarının değerlerini değiştirerek gerçekleştirilen özel uygulama gereksinimlerine göre ayarlanabilir veya ayarlanmış olduğu gerçeğini ifade eder. Değişken çentik filtresi ayarlanabilir bir özelliğe sahiptir ve frekans filtreleme özelliklerinden daha geniş bir aralıkta yararlanmamızı sağlar, bu nedenle farklı hız aralıkları için kayan mod gözlemci kontrolünde hata azaltma amacına ulaşmada ana rol oynar.

Simülasyon üç ana bölümden oluşmaktadır: İnvertör ve IPMSM, akım kontrol bloğu ve hız kontrol bloğu, bu tezde ana odak noktası kayan mod gözlemcisi ve akım kontrol bloğundaki değişken çentik filtresidir. Geleneksel kayan kipli gözlemci kontrolü ile IPMSM'nin hızı ve konumu tahmin edilip hesaplandıktan sonra, değişken çentik filtresi kullanılarak önerilen yöntem sisteme uygulanmıştır. çentik filtresi ile herhangi bir değişiklik yapılmadan önce bir alçak geçiren filtre ve bir DC bileşen giderme bloğu kullanılmıştır. bu blok için alçak geçiren katsayısı 0,005 veya daha kesin olarak (0,005x(T_s/50e-6)) olarak ayarlanmıştır.

IPMSM parametrelerinin önceden tanımlandığı bu durumda, 0.1 pu referans hızı için salınan frekans 27.34 Hz olan sinyalin FFT analizinden elde edilir.

Önerilen yöntem MATLAB®/Simulink®'te simüle edildikten ve yukarıda bahsedilen frekans tahmin edilen hızdan filtrelendikten sonra, sinyalin birinci harmonik salınımında önemli bir azalma sağlanmış ve FFT frekans yanıtına göre, motor 0,1 pu'da dönerken genliği 0,14'ten 0,05'e düşürülmüştür.

Referans hız 0,5 olduğunda tahmin edilen hızın FFT analizi sunulmuştur ve iki ana frekans veya salınım olduğunu görebilirsiniz. Biri yaklaşık 13 Hz ve diğeri 137

Hz'dir. Bu iki frekansı ortadan kaldırmak için, mevcut çalışmada araştırılmamış olan çift çentikli filtre önerilmektedir. Gelecekteki çalışmalarda çift veya çoklu çentik filtreleri düşünülebilir. Konfigürasyonu 13 Hz olarak ayarlanan tek bir çentik filtresi uygulandığında, yukarıda bahsedilen frekansın genliği $5{,}25\times10^{-3}$'den $3{,}4\times10^{-3}$'e düşmektedir. Dolayısıyla, daha yüksek hızlarda, örneğin 0,5 pu, hız tahmin sinyalinin frekans yanıtında iki ana harmonik vardır, bu nedenle SMO yönteminde gevezeliği azaltmak için her ikisi de ortadan kaldırılmalıdır. Çift çentikleme, herhangi bir hız aralığında tüm istenmeyen frekansları ortadan kaldırabilen bu çalışmanın bir sonraki nesli olabilir.

Buna karşılık, daha yüksek frekansın (137 Hz) zayıflatılmasının da faydaları vardır. Bu durumda hatanın genliği azalır ancak kalan frekansın yüksek genliği nedeniyle tahmini hatadaki azalma yeterli değildir.

Sonuç olarak, bu yöntem sistemdeki salınımı azaltmış ve frekansı zayıflatarak tahmin hatasının azaltılmasına yol açmış, IPMSM'nin konum algılamasının sağlamlığını ve doğruluğunu artırmıştır.

1. INTRODUCTION

1.1 Objectives and Scope of the Thesis

A detailed analysis of the previous methods is explained, and applicable methods for reducing the estimated position error are introduced. The contribution related to this topic is about the accuracy of estimation by employing a variable notch filter both in speed and position estimation with regard to the reference speed frame.

1.2 Outline of Thesis

This thesis is considered as the form of a "compilation thesis"; therefore, some of the main concepts have been explained to provide a brief background regarding the scientific contribution. Those topics have been presented as follows: Chapter 2 contains a brief review of modeling IPMSM and its parameters which would be used in the equations of the proposed method. Then alpha-beta and D-Q reference frame transformation has been discussed, which are used excessively in the Simulink. Chapter 3 includes different methods for sensorless control and mathematical equations for the sliding mode observer control. Chapter 4 is an overview of the notch filter. The transfer function for the variable notch filter is extracted and explained, and finally, its effectiveness for the sensorless control is presented. Chapter 5 focuses on the Simulink part of the thesis and depicts the reduced error position for the proposed method, and the error is compared to the conventional method. The response of the whole system under different conditions, such as applying pulse torque, speed change, and etc., are presented. Chapter 6 concludes all aforementioned topics in previous chapters and provides a wider vision of the proposed method for further research areas.

1.3 Scientific Contribution

Harmonics are inevitable parameters of a nonlinear system where in IPMSM control, nonlinearity is generated by the non-ideal inverter, the existence of dead time in the

inverter, flux spatial linkage, and parameter variations. In the case of SMO sensorless control, these harmonics affect the estimation, and the estimated speed and position fluctuate in relation to the frequency of the rotor rotation. In order to mitigate this fluctuation which increases the error rate in the system, a variable notch filter is suggested. Utilizing this filter benefits us by eliminating the desired harmonic, which is in relation to the rotation frequency.

A notch filter is described in Chapter 4, and simulating the system and explaining the coefficient parameters are presented in Chapter 5.

1.4 Literature Review

Open loop and close loop control methods for PMSM are explained. In the open loop control method, the exact position of the rotor is not needed and controlling a motor at a precisely desired speed is not possible. Controlling motor for the close loop is categorized into two methods, first receiving shaft position data from a physical, mechanical, or electromechanical sensor and second, estimating the position of the rotor without the presence of sensors by utilizing the current and voltage information extracted from the stator parameters [1]. Second-order disturbance observer for nonlinear systems was explained, and an active flux is used for position estimation [2]. Back EMF estimation was not satisfying in comparison to the flux component in [2], and the quadrature phase-locked loop method is suggested and claimed to be suitable for ramp frequency.

Sliding observer mode has some defects and it is not a flawless method. chattering is one of the disadvantageous of the sliding mode observer methods [3]. In order to solve this problem, a Fast Terminal SMO Control is suggested in [4] which improves response time. it is also recommended to use an S function instead of a sharp sign function [5]. Load and temperature instability affects the flux linkage in actual operation, which influences the estimation accuracy; therefore, filtering and choosing a proper compensatory method is crucial. In [6] arc-hyperbolic sine function-based method for improving SMO performance is presented, and fast vector selection has been chosen to reduce the torque ripples. Lyapunov stability conditions are satisfied to enhance the anti-reference mechanism of the system. The Lyapunov stability condition provides a

way to determine whether a particular equilibrium point of a dynamical system is stable or not. Thus, small perturbations around that point will eventually decay or unstable.

In [7], high-speed position estimation strategies are presented. Observers which are designed for sensorless estimation include disturbance and high-frequency switching to increase the accuracy of the process and estimation. Multi-harmonic elimination is explained widely in [7], where several band-pass filters are used to distinguish fundamental frequencies, and several band-stop filters are used to eliminate distorted harmonics. Therefore, they have proposed a comb filter which is suitable for that purpose. Under non-ideal conditions, the nonlinear behaviour of the system, sampling limitation, probable inaccuracy in voltage and current measurement, and variation in time for some parameters should be taken into consideration.

An adaptive filter for increasing and improving the performance of IPMSM by applying using recursive-least-square method is presented in [8], and the fifth and seventh harmonic analysis, which is caused by inverters' nonlinearity, is done. The estimated position error is attenuated with an adaptive filter (AF) under the sliding mode observer (SMO) control method. In [9] position, harmonic errors are analyzed and fifth and seventh harmonics, which are caused by the dead-time effect and the system's nonlinearity, are discussed. The magnitude of the other harmonics is so low. Hence they are negligible, and the main reasons for estimation error are the fifth and seventh harmonics.

In [10] reference frame phase lock loop is proposed, which is also called dq0-PLL. dq0-PLL is not suitable for unbalanced inputs due to its double frequency error. Diminishing this defect is possible by adding a low-pass filter in the loop or in the system's pre-loop; on the other hand, eliminating low frequencies with an LPF affects its dynamic, and a huge bandwidth reduction will occur. DC components are inseparable components of a signal which can be caused by dc-link voltage or saturation of measurement devices. [11]. In [12], enhanced PLL is presented, and it can work in variable frequencies. Meanwhile, a power frequency estimator is proposed in In [12]. An input low-frequency range (10 Hz to 100 Hz) can be estimated only in a few cycles with a steady-state error of around 20 MHz.

The estimated frequency will be utilized in regulating the coefficients of the notch filter used in the proposed method. In [13] SMO method is explained, and back EMF is used to estimate the position of an IPMSM, in which the sigmoid function is chosen instead of the conventional sign function to increase the robustness of the system and by eliminating all filters, an adaptive line enhancer is utilized instead.

In [14], discrete SMO with ATO or inverse tangent is presented for IPMSM. Speed feedback is employed to improve ATO, the error for this case was ±3 electrical degrees with a sampling frequency of around 6 kHz.

In [15], a reference frame filter technique is used to improve SMO. The stator voltage vector is converted to d-axis signals, and then LPF is applied to the aforementioned signal; it should be considered that LPF doesn't have any effect on the d-axis of the current. Therefore, its impact is completely negligible.

2. IPMSM

2.1 Outline of Chapter

In this chapter, reference frame transformations, three-phase to an orthogonal stationary reference frame (Clarke, abc to $\alpha - \beta$) and orthogonal stationary reference frame to rotating reference frame (Park, $\alpha - \beta$ to d-q) is discussed in section 2.2 and mathematical transformation is explained. Then, a short explanation and mathematical model of IPMSM are presented in section 2.3, and finally, in Section 2.4, control methods of IPMSM are explained.

2.2 Clarke and Park Transformation

The response of three-phase machines is typically defined by the characteristic of the current and voltage equation. The differential equation of those parameters varies while the machine is performing unless it has been set to zero speed. Due to an incessant change of induced voltage, and flux linkage caused by rotation, mathematical modeling of such a system is a hardship. To overcome that obstacle, all variables, including time variable parameters, are transformed to a common reference frame to avoid complexity. The most common and practical transformations for electric machines are:

- Clarke transformation
- Park transformation

In this section, Clarke, Park, inverse Park and inverse Clarke will be explained.

2.2.1 Clarke transformation

In Clarke transformation, three-phase parameters i_a, i_b and i_c are transformed to a two-axis stationary orthogonal i_α, i_β and i_γ frame. Vector diagram of Clarke transformation is shown in Figure 2.1.

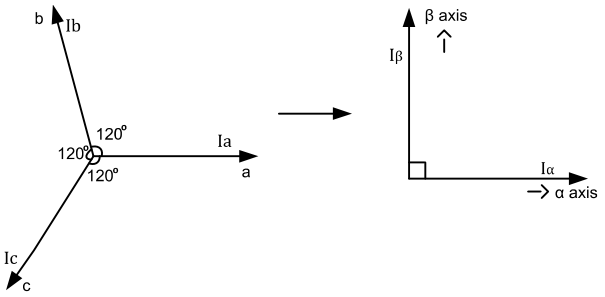

Figure 2.1 : Vector diagram of Clarke transformation

The equation for Clarke transformation is as follows:

$$i_\alpha = \frac{2}{3} i_a - \frac{1}{3}(i_b - i_c) \tag{2.1}$$

$$i_\beta = \frac{2}{\sqrt{3}}(i_b - i_c) \tag{2.2}$$

$$i_\gamma = \frac{2}{3}(i_a + i_b + i_c) \tag{2.3}$$

Where:

i_a, i_b and i_c are three-phase parameters, and

i_α, i_β and i_γ are the stationary frame parameters.

In a symmetric manner, $i_a + i_b + i_c$ is equal to zero, therefore the quantity for the third parameter (i_γ) is zero in Equation 2.3 which is negligible in our calculation, thus Equation 2.1 and Equation 2.2 are written as follow:

$$I_\alpha = I_a \tag{2.4}$$

$$I_\beta = \frac{1}{\sqrt{3}}(I_a + 2I_b) \tag{2.5}$$

2.2.2 Inverse clarke transformation

Inverse Clarke transformation is used to change the reference frame from a two-axis orthogonal frame to a three-axis one, which is presented as follows:

$$i_a = i_\alpha \tag{2.6}$$

$$i_b = -\frac{1}{2} i_\alpha + \frac{\sqrt{3}}{2} i_\beta \tag{2.7}$$

$$i_c = -\frac{1}{2} i_\alpha - \frac{\sqrt{3}}{2} i_\beta \tag{2.8}$$

Both Clarke and inverse Clarke transformations can be written in a matrix format which is shown in Equation 2.9 and Equation 2.10, respectively:

$$\begin{bmatrix} i_\alpha \\ i_\beta \end{bmatrix} = \sqrt{\frac{2}{3}} \begin{bmatrix} 1 & -1/2 & -1/2 \\ 0 & \sqrt{3}/2 & -\sqrt{3}/2 \end{bmatrix} \begin{bmatrix} i_a \\ i_b \\ i_c \end{bmatrix} \tag{2.9}$$

$$\begin{bmatrix} i_a \\ i_b \\ i_c \end{bmatrix} = \sqrt{\frac{2}{3}} \begin{bmatrix} 1 & 0 \\ -1/2 & \sqrt{3}/2 \\ -1/2 & -\sqrt{3}/2 \end{bmatrix} \begin{bmatrix} i_\alpha \\ i_\beta \end{bmatrix} \tag{2.10}$$

2.2.3 Park transformation

Alpha-beta reference frame is transformed to a rotating reference (d-q) by using park transformation [16], which is presented in Equation 2.11 and Equation 2.12. Vector diagram of Park transformation is shown in Figure 2.2.

$$I_d = I_\alpha \cdot \cos(\theta) + I_\beta \cdot \sin(\theta) \tag{2.11}$$

$$I_q = I_\beta \cdot \cos(\theta) - I_\alpha \cdot \sin(\theta) \tag{2.12}$$

2.2.4 Inverse park transformation

Inverse park transformation is employed to convert direct and quadrature parameters of the d-q reference frame to stationary $\alpha - \beta$ reference frame. The equations for this transformation, when the d-axis and α-axis are aligned, are shown in Equation 2.13 and Equation 2.14.

$$i_\alpha = i_d \cdot \cos(\theta) - i_q \cdot \sin(\theta) \tag{2.13}$$

$$i_\beta = i_d \cdot \sin(\theta) + i_q \cdot \cos(\theta) \tag{2.14}$$

Both Clarke and inverse Clarke transformations can be written in a matrix format which is shown in Equation 2.15 and Equation 2.16, respectively.

$$\begin{bmatrix} i_d \\ i_q \end{bmatrix} = \begin{bmatrix} \cos\theta & \sin\theta \\ -\sin\theta & \cos\theta \end{bmatrix} \begin{bmatrix} i_\alpha \\ i_\beta \end{bmatrix} \tag{2.15}$$

$$\begin{bmatrix} i_\alpha \\ i_\beta \end{bmatrix} = \begin{bmatrix} \cos\theta & -\sin\theta \\ \sin\theta & \cos\theta \end{bmatrix} \begin{bmatrix} i_d \\ i_q \end{bmatrix} \tag{2.16}$$

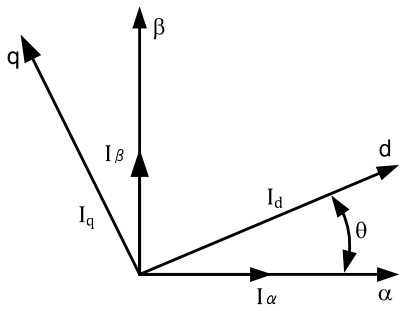

Figure 2.2 : Vector diagram of Park transformation

2.3 Modeling IPMSM

2.3.1 Overall description of IPMSM

The first general introduction revolves around IPMSM, then the difference between two types of PMSM is discussed, and finally, equations and mathematical modeling of IPMSM are explained in a three-phase stationary reference frame, $\alpha - \beta$ orthogonal stationary frame and a rotating (d-q) reference frame.

Like all other rotating electric motors, a permanent magnet synchronous motor is made up of a rotor and a stator which the fixed component is named as stator and the rotating component is the rotor; components of IPMSM are shown in Figure2.3 [17]. A synchronous motor's mechanism principle is based on the interaction between the rotor's constant magnetic field and the stator's rotating magnetic field and thanks to Ampere's law, torque is generated so the rotor starts to rotate. According to studies, [18] efficiency of PMSM is almost 12% higher than induction machine under the same applied frequency and stator structure; thus, it is widely used thanks to high efficiency, high torque-current ratio and large power density in a wide range of speed. Therefore it can be a good option to be used in robots, railways, aerospace and home appliances. Rotor has permanent magnets with high coercive force, and the position of these magnets categorizes PMSM as:

- Salient pole rotor
- Non-salient pole rotor

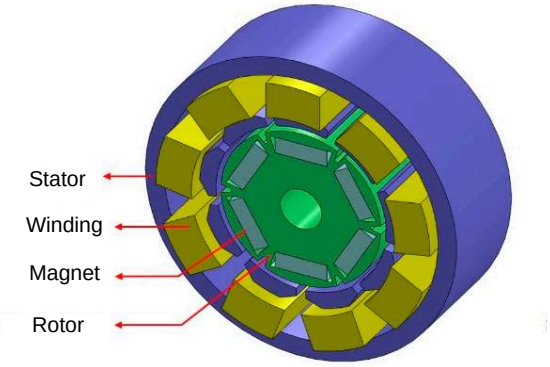

Figure 2.3 : Components of interior permanent magnet synchronous motor [17].

Non-salient pole PMSM has a symmetrical structure; therefore, due to this reason, inductance in the direct and quadrature axis of PMSM is the same, conversely structure and shape of salient pole PMSM affects those two axes, and inductance is not the same in both axis, where d-axis inductance is expected to be less than the q-axis in most cases. d-q reference frame transformation is thoroughly explained in Section 2.2. Different structures of the salient pole PMSM and their representative d-q axis inductance are shown in Figure 2.4.

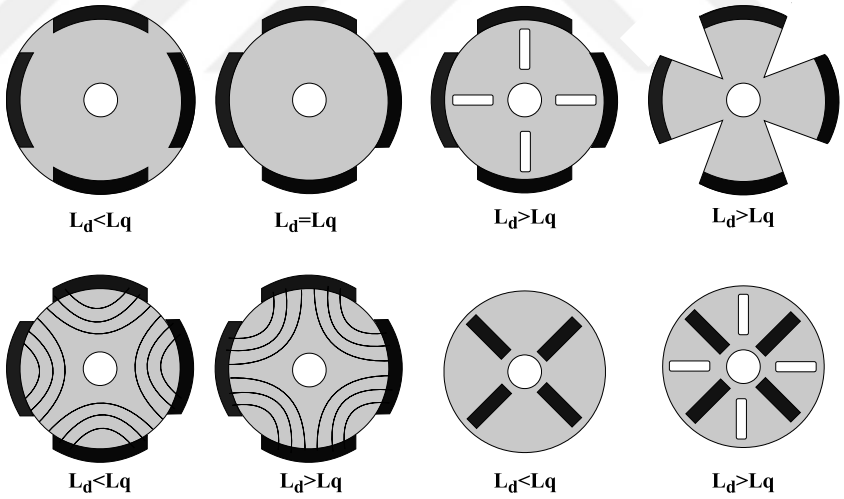

Figure 2.4 : Structures of salient pole PMSM with different d-q axis inductance.

2.3.2 Mathematical modeling of IPMSM

Voltage equation in the three-phase coordination for IPMSM written as: [19] [20]

$$\begin{bmatrix} v_{as} \\ v_{bs} \\ v_{cs} \end{bmatrix} = R_s \begin{bmatrix} i_{as} \\ i_{bs} \\ i_{cs} \end{bmatrix} + p \begin{bmatrix} \lambda_{as} \\ \lambda_{bs} \\ \lambda_{cs} \end{bmatrix} \tag{2.17}$$

R_s is the winding resistance, and subtle resistance difference between phases is neglected and is considered the same for all phases. The flux linkage equation is as follows: Equation 2.18

$$\begin{bmatrix} \lambda_{as} \\ \lambda_{bs} \\ \lambda_{cc} \end{bmatrix} = L_{abc} \begin{bmatrix} i_{\text{as}} \\ i_{bs} \\ i_{cs} \end{bmatrix} + \begin{bmatrix} \lambda_{ma} \\ \lambda_{mb} \\ \lambda_{mc} \end{bmatrix} \tag{2.18}$$

In Equation 2.18, λ_{ma}, λ_{mb}, and λ_{mc} are permanent magnet flux of phase a,b,and c [21].

For L_{abc} (stator inductance) we have:

$$L_{abc} = \begin{bmatrix} L_{aa} & L_{ab} & L_{ac} \\ L_{ba} & L_{bb} & L_{bc} \\ L_{ca} & L_{cb} & L_{cc} \end{bmatrix} \tag{2.19}$$

Self inductance and mutual inductance for Equation 2.19 is expressed from Equation 2.20 to Equation 2.25

$$L_{aa} = L_{sr} + L_{sl} - L_{g2}\cos 2\theta_r \tag{2.20}$$

$$L_{bb} = L_{sr} + L_{sl} - L_{g2}\cos 2\left(\theta_r - \frac{2}{3}\pi\right) \tag{2.21}$$

$$L_{cc} = L_{sr} + L_{sl} - L_{g2}\cos 2\left(\theta_r + \frac{2}{3}\pi\right) \tag{2.22}$$

$$L_{ab} = L_{ba} = -\frac{1}{2}L_{sr} - L_{g2}\cos 2\left(\theta_r - \frac{\pi}{3}\right) \tag{2.23}$$

$$L_{bc} = L_{cb} = -\frac{1}{2}L_{sr} - L_{g2}\cos 2\theta_r \tag{2.24}$$

$$L_{ac} = L_{ca} = -\frac{1}{2}L_{sr} - L_{g2}\cos 2\left(\theta_r + \frac{\pi}{3}\right) \tag{2.25}$$

The rotor PM flux for each phase is written as:

$$\begin{bmatrix} \lambda_{ma} \\ \lambda_{mb} \\ \lambda_{mc} \end{bmatrix} = \begin{bmatrix} \cos\theta_r \\ \cos\left(\theta_r - \frac{2}{3}\pi\right) \\ \cos\left(\theta_r + \frac{2}{3}\pi\right) \end{bmatrix} \lambda_m \tag{2.26}$$

By merging Equation 2.18 to Equation 2.26, flux equation can be written as:

$$\begin{bmatrix} \lambda_{as} \\ \lambda_{bs} \\ \lambda_{\text{bs}} \end{bmatrix} = \left(L_{sl} + \frac{3}{2}L_{sr}\right) \begin{bmatrix} i_{as} \\ i_{bs} \\ i_{cs} \end{bmatrix} - L_c \begin{bmatrix} i_{as} \\ i_{bs} \\ i_{cs} \end{bmatrix} + \begin{bmatrix} \cos\theta_r \\ \cos\left(\theta_r - \frac{2}{3}\pi\right) \\ \cos\left(\theta_r + \frac{2}{3}\pi\right) \end{bmatrix} \lambda_m \tag{2.27}$$

Where:

$$L_c = L_{\text{g2}} \begin{bmatrix} \cos 2\theta_r & \cos 2\left(\theta_r - \frac{\pi}{3}\right) & \cos 2\left(\theta_r + \frac{\pi}{3}\right) \\ \cos 2\left(\theta_r - \frac{\pi}{3}\right) & \cos 2\left(\theta_r + \frac{\pi}{3}\right) & \cos 2\theta_r \\ \cos 2\left(\theta_r + \frac{\pi}{3}\right) & \cos 2\theta_r & \cos 2\left(\theta_r - \frac{\pi}{3}\right) \end{bmatrix} \tag{2.28}$$

For the stationary $\alpha\beta$ reference frame voltage equation can be expressed as:

$$\begin{bmatrix} v_{\alpha s} \\ v_{\beta s} \\ v_{0s} \end{bmatrix} = R_s \begin{bmatrix} i_{\alpha s} \\ i_{\beta s} \\ i_{0s} \end{bmatrix} + p \begin{bmatrix} \lambda_{\alpha s} \\ \lambda_{\beta s} \\ \lambda_{0\mathrm{s}} \end{bmatrix} \tag{2.29}$$

and

$$\begin{bmatrix} \lambda_{\alpha s} \\ \lambda_{\beta s} \\ \lambda_{0s} \end{bmatrix} = L_{\alpha\beta 0} \cdot \begin{bmatrix} i_{\alpha s} \\ i_{\beta s} \\ i_{0s} \end{bmatrix} + \begin{bmatrix} \lambda_{m\alpha} \\ \lambda_{m\beta} \\ \lambda_{m0} \end{bmatrix} \tag{2.30}$$

Where:

$$L_{\alpha\beta 0} = \begin{pmatrix} L_{sl} + \frac{3}{2}\left(L_{sr} - L_{g2}\cos 2\theta_r\right) & \frac{3}{2}L_{g2}\sin 2\theta_r & 0 \\ \frac{3}{2}L_{g2}\sin 2\theta_r & L_{sl} + \frac{3}{2}\left(L_{sr} + L_{g2}\cos 2\theta_r\right) & 0 \\ 0 & 0 & L_{sl} \end{pmatrix} \tag{2.31}$$

Stator flux and voltage is represented in Equation 2.32 and Equation 2.33 respectively:

$$\begin{bmatrix} \lambda_{\alpha s} \\ \lambda_{\beta s} \end{bmatrix} = \begin{bmatrix} L_{sl} + \frac{3}{2}L_{sr} - \frac{3}{2}L_{g2}\cos 2\theta_r & \frac{3}{2}L_{g2}\sin 2\theta_r \\ \frac{3}{2}L_{g2}\sin 2\theta_r & L_{sl} + \frac{3}{2}L_{sr} + \frac{3}{2}L_{g2}\cos 2\theta_r \end{bmatrix} \begin{bmatrix} i_{\alpha s} \\ i_{\beta s} \end{bmatrix} + \begin{bmatrix} \cos\theta_r \\ \sin\theta_r \end{bmatrix} \lambda_m \tag{2.32}$$

$$\begin{bmatrix} v_{\alpha s} \\ v_{\beta s} \end{bmatrix} = \begin{bmatrix} r_s + pL_\alpha & pL_{\alpha\beta} \\ pL_{\alpha\beta} & r_s + pL_\beta \end{bmatrix} \begin{bmatrix} i_{\mathrm{as}} \\ i_{\beta s} \end{bmatrix} + \begin{bmatrix} -\sin\theta_{re} \\ \cos\theta_{re} \end{bmatrix} \lambda_m \tag{2.33}$$

The voltage equation in the d-q axis is shown in Equation 2.34 [22].

$$\begin{bmatrix} v_{ds} \\ v_{qs} \end{bmatrix} = R_s \begin{bmatrix} i_{ds} \\ i_{qs} \end{bmatrix} + \frac{d}{dt} \begin{bmatrix} \lambda_{ds} \\ \lambda_{qs} \end{bmatrix} - \omega_r \begin{bmatrix} \lambda_{qs} \\ -\lambda_{ds} \end{bmatrix} \tag{2.34}$$

Flux is:

$$\begin{bmatrix} \lambda_{ds} \\ \lambda_{qs} \end{bmatrix} = L_{dq} \begin{bmatrix} i_{ds} \\ i_{qs} \end{bmatrix} + \begin{bmatrix} 1 \\ 0 \end{bmatrix} \lambda_m \tag{2.35}$$

Inductance is:

$$L_{dq} = \begin{bmatrix} \frac{3}{2}\left(L_{sr} - L_{g2}\right) + L_{sl} & 0 \\ 0 & \frac{3}{2}\left(L_{sr} + L_{g2}\right) + L_{sl} \end{bmatrix} = \begin{bmatrix} L_d & 0 \\ 0 & L_q \end{bmatrix} \tag{2.36}$$

From Equation 2.36, L_d and L_q can be written:

$$L_d = \frac{3}{2}\left(L_{sr} - L_{g2}\right) + L_{sl} \tag{2.37}$$

$$L_q = \frac{3}{2}\left(L_{sr} + L_{g2}\right) + L_{sl} \tag{2.38}$$

The voltage equation in the dq frame is:

$$\begin{bmatrix} v_{ds} \\ v_{qs} \end{bmatrix} = \begin{bmatrix} r_s + L_d p & 0 \\ 0 & r_s + L_q p \end{bmatrix} \begin{bmatrix} i_{ds} \\ i_{qs} \end{bmatrix} + \omega_r \begin{bmatrix} -L_q i_{qs} \\ L_d i_{ds} + \lambda_m \end{bmatrix} \tag{2.39}$$

Equation 2.40 can be derived from Equation 2.28. Relation between L_q and L_d with the abc and $\alpha\beta$ is shown in Equation 2.40) and Equation 2.41

$$\begin{bmatrix} \lambda_{as} \\ \lambda_{bs} \\ \lambda_{cs} \end{bmatrix} = \frac{L_d + L_q}{2} \begin{bmatrix} i_{\text{as}} \\ i_{\text{bs}} \\ i_{cs} \end{bmatrix} - \frac{L_q - L_d}{2} \cdot \frac{L_c}{L_{g2}} \begin{bmatrix} i_{as} \\ i_{bs} \\ i_{cs} \end{bmatrix} + \begin{bmatrix} \cos\theta_r \\ \cos\left(\theta_r - \frac{2}{3}\pi\right) \\ \cos\left(\theta_r + \frac{2}{3}\pi\right) \end{bmatrix} \lambda_m \tag{2.40}$$

$$\begin{bmatrix} \lambda_{\alpha s} \\ \lambda_{\beta s} \end{bmatrix} = L_{\alpha\beta} \begin{bmatrix} i_{as} \\ i_{\beta s} \end{bmatrix} + \begin{bmatrix} -\sin\theta_r \\ \cos\theta_r \end{bmatrix} \lambda_m \tag{2.41}$$

Where $L_{\alpha\beta}$ is:

$$\begin{bmatrix} r_s + p\left(\frac{L_d+L_q}{2} + \frac{L_d-L_q}{2}\cos 2\theta\right) & p\left(\frac{L_d-L_q}{2}\sin 2\theta\right) \\ p\left(\frac{L_d-L_q}{2}\sin 2\theta\right) & r_s + p\left(\frac{L_d+L_q}{2} - \frac{L_d-L_q}{2}\cos 2\theta\right) \end{bmatrix} \tag{2.42}$$

2.4 Control of IPMSM

The control of IPMSMs is similar to that of other PMSMs, but there are some differences due to the unique characteristics of the IPMSM.

One of the main differences in the control of IPMSMs is the need to account for the magnetic field generated by the permanent magnets inside the rotor. This can be done using a mathematical model of the motor that includes the rotor magnetization distribution and the magnetic permeability of the rotor material. The model can then be used to design a control algorithm that takes into account the magnetic field distribution and minimizes torque ripple.

2.4.1 Open-loop control

Open-loop control is a simple and less complex control strategy where the control inputs (such as voltage or current) are set based on the desired speed and torque without any feedback. The control algorithm assumes that the motor is behaving exactly as expected without taking into account any disturbances or external factors that may affect the motor's performance. Therefore, open-loop control is generally less accurate and less robust, and another defect is vulnerability against sudden load change in the synchronous speed. [23]

2.4.2 Close-loop control

closed-loop control (also known as feedback control) uses feedback from the motor's current, voltage, and speed sensors to adjust the control inputs in real time and

compensate for any disturbances or external factors. The control algorithm continuously measures the motor's actual speed and torque and compares it to the desired values, then adjusts the control inputs to minimize the error. The main advantage of closed-loop control is its ability to compensate for disturbances and uncertainties, leading to improved accuracy, stability, and robustness. This makes it a preferred choice for applications where precise speed and torque control is required, such as in robotics, industrial automation, and electric vehicles.

In closed-loop control, the feedback loop is implemented by using a proportional-integral-derivative (PID) controller. The values of PID feedback control method parameters or coefficients depend on the specific requirements of the application and the motor's dynamic characteristics.

There are several types of closed-loop control techniques used for IPMSMs. Some common types of closed-loop control for IPMSMs are explained in Section 2.4.2.1 to 2.4.2.5.

2.4.2.1 Speed control

This is the most basic type of closed-loop control, where the motor's speed is measured using a speed sensor and compared to the desired speed setpoint. The control algorithm then adjusts the control inputs (such as voltage or current) to minimize the speed error. The most commonly used method for speed control is a proportional-integral-derivative (PID) controller.

2.4.2.2 Torque control

This type of control is used when the torque output of the motor is more critical than the speed [22]. In this case, the control algorithm measures the motor's torque using a torque sensor or by estimating it from the motor's current and voltage measurements, then adjusts the control inputs to minimize the torque error [24].

2.4.2.3 Field-oriented control (FOC)

FOC is a more advanced type of closed-loop control that involves transforming the three-phase stator currents and voltages into a two-axis reference frame, where the d-axis is aligned with the rotor magnetic field and the q-axis is perpendicular to it [25].

The control system then regulates the d-axis and q-axis currents to achieve the desired torque and speed. FOC provides better control performance and reduces torque ripple [26–28].

2.4.2.4 Direct torque control (DTC)

The principle of DTC is to directly control the torque and stator flux by selecting the appropriate voltage vector from a predefined lookup table based on the measured motor's state. The control algorithm employs a hysteresis band around the desired torque and flux values to switch between the voltage vectors. The voltage vector is chosen in such a way that it produces the desired torque and flux while minimizing the torque ripple and stator current harmonics [29].

2.4.2.5 Model predictive control (MPC)

MPC is a more complex type of closed-loop control that uses a mathematical model of the motor to predict its behavior and optimize the control inputs to achieve the desired performance. MPC can provide better performance than PID control and is suitable for applications where fast and accurate control is required [26].

3. SENSORLESS CONTROL

3.1 Outline of Chapter

In this chapter, control strategies in sensorless control are explained, then in section 3.1.2, theatrical and mathematical explanation of sliding mode observer control is explained where the equation for estimating the speed and position of the rotor is presented and SMO in $\alpha - \beta$ and d-q reference frame is discussed in section 3.1.2.1 and 3.1.2.2

3.1.1 Principle of sensorless control

Controlling IPMSM is categorized into two sections; an open-loop strategy in which the essence of shaft position information is not needed, and a close-loop strategy in which the shaft's position information is required and is subdivided into two methods: 1. Sensored and 2. Sensorless [1].

There are three methods for rotor position estimation. The first one is fundamental excitation which includes adaptive [30] and non-adaptive methods. Secondly, signal injection methods [31] [32], and the last one is the help of artificial intelligence.

Adaptive methods are categorized as model reference adaptive base systems, and observer-based control, which is subdivided into Luenberger Observer, reduced order observer, sliding mode observer, and Kalman filter. In this work, a sliding mode observer is employed, and the error in this method is reduced by applying varying notch filters in the system. Finally, there is a minimum square error estimator taking place in this category.

The non-adaptive method consists of estimators which they utilize stator current and voltage, estimators based on flux, and estimators which rely on back EMF.

Signal injection methods are used in salient motors in which the quantity of inductance in the direct and quadrature axis are not the same. Hence it is utilized to estimate the

position of the rotor. High-frequency and low-frequency signals are injected into the stator's voltage or current to get the corresponding parameter to estimate the position.

The last category is the artificial intelligence method which includes fuzzy neural networks and fuzzy logic-based methods.

3.1.2 Sliding mode observer

The following equation is derived from Equation 2.29 and Equation 2.30.

$$\frac{d}{dt}\begin{bmatrix} i_{s\alpha} \\ i_{s\beta} \\ e_{s\alpha} \\ e_{s\beta} \end{bmatrix} = \begin{bmatrix} -\frac{R_s}{L_s} & 0 & -\frac{1}{L_s} & 0 \\ 0 & -\frac{R_s}{L_s} & 0 & -\frac{1}{L_s} \\ 0 & 0 & 0 & -\omega_e \\ 0 & 0 & \omega_e & 0 \end{bmatrix} \cdot \begin{bmatrix} i_{s\alpha} \\ i_{s\beta} \\ e_{s\alpha} \\ e_{s\beta} \end{bmatrix} + \begin{bmatrix} \frac{1}{L_s} & 0 \\ 0 & \frac{1}{L_s} \\ 0 & 0 \\ 0 & 0 \end{bmatrix} \cdot \begin{bmatrix} u_{s\alpha} \\ u_{s\beta} \end{bmatrix} \tag{3.1}$$

Equation 3.1 is used for the case where the difference and variance between the d and q axis are not so significant.

For simplicity Equation 3.1 can be written as:

$$\frac{d}{dt}\begin{bmatrix} i_{s(\alpha,\beta)} \\ \hat{e}_{s(\alpha,\beta)} \end{bmatrix} = \begin{bmatrix} A_{11} & A_{12} \\ 0 & A_{22} \end{bmatrix} \cdot \begin{bmatrix} i_{s(\alpha,\beta)} \\ \hat{e}_{s(\alpha,\beta)} \end{bmatrix} + \begin{bmatrix} B_1 \\ 0 \end{bmatrix} \cdot \left[u_{s(\alpha,\beta)}\right] \tag{3.2}$$

Where:

$$A_{11} = a_{11} \cdot I = -\frac{R_S}{L_S} \cdot I \tag{3.3}$$

$$A_{12} = a_{12} \cdot I = -\frac{1}{L_S} \cdot I \tag{3.4}$$

$$A_{22} = a_{22} \cdot J = \omega_e \cdot J \tag{3.5}$$

$$B_1 = b_1 \cdot I = -a_{12} \cdot I = \frac{1}{L_S} \cdot I \tag{3.6}$$

and,

$$I = \begin{bmatrix} 1 & 0 \\ 0 & 1 \end{bmatrix} \tag{3.7}$$

$$J = \begin{bmatrix} 0 & -1 \\ 1 & 0 \end{bmatrix} \tag{3.8}$$

Sliding mode observer is based on feedback from a sign function, and the estimated value of $\hat{e}_{s(\alpha,\beta)}$ can be derived from the equation below:

$$\frac{d}{dt}\begin{bmatrix} \hat{i}_{s(\alpha,\beta)} \\ \hat{e}_{s(\alpha,\beta)} \end{bmatrix}(t) = C + K_1 \cdot \begin{bmatrix} I \\ G \end{bmatrix} \cdot sgn\left(\hat{i}_{s(\alpha,\beta)}(t) - i_{s(\alpha,\beta)}(t)\right) \tag{3.9}$$

Where C is:

$$C = \begin{bmatrix} A_{11} & A_{12} \\ 0 & A_{22} \end{bmatrix} \cdot \begin{bmatrix} \hat{i}_{s(\alpha,\beta)} \\ \hat{e}_{s(\alpha,\beta)} \end{bmatrix}(t) + \begin{bmatrix} B_1 \\ 0 \end{bmatrix} \cdot \left[\hat{u}_{s(\alpha,\beta)}\right](t) \tag{3.10}$$

Coefficients $A_{11}, A_{12}, A_{22}, B_1$ are in Equation 3.3) to Equation 3.6

Sgn vector is defined as the function below:

$$\text{sgn}\left(\begin{bmatrix} i_\alpha \\ i_\beta \end{bmatrix}\right) = \begin{bmatrix} sgn_\alpha = 1 \Leftrightarrow i_\alpha > 0, sgn_\alpha = 0 \Leftrightarrow i_\alpha = 0, sgn_\alpha = -1 \Leftrightarrow i_\alpha < 0 \\ sgn_\beta = 1 \Leftrightarrow i_\beta > 0, sgn_\beta = 0 \Leftrightarrow i_\beta = 0, sgn_\beta = -1 \Leftrightarrow i_\beta < 0 \end{bmatrix} \tag{3.11}$$

For better performance and chattering reduction, the sign function can be replaced with the S-function [33–35] which is shown in Figure 3.1, and the represented equation is as follows: Equation 3.12

$$\begin{bmatrix} \Gamma_\alpha \\ \Gamma_\beta \end{bmatrix} = \begin{bmatrix} \Gamma\left(\hat{i}_\alpha - i_\alpha\right) \\ \Gamma\left(\hat{i}_\beta - i_\beta\right) \end{bmatrix} = \begin{bmatrix} \frac{1}{1+\exp\left[-n\left(\hat{i}_\alpha - i_\alpha\right)\right]} - \frac{1}{2} \\ \frac{1}{1+\exp\left[-n\left(\hat{i}_\beta - i_\beta\right)\right]} - \frac{1}{2} \end{bmatrix} \tag{3.12}$$

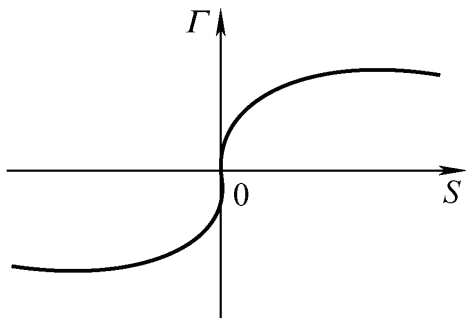

Figure 3.1 : S function used in SMO.

Feedback and switching gains are presented in Equation (3.13) and Equation 3.14, respectively.

$$G = g_1 \cdot I + g_2 \cdot J \tag{3.13}$$

$$K_1 = k_1 \cdot I \tag{3.14}$$

The geometrical value of θ is needed for the purpose of vector control, and the sine and cosine quantity of this parameter can be calculated from the equations below: Equation 3.30 and Equation 3.31

$$\cos(\theta) = \frac{e_{s\alpha}}{\sqrt{\left(e_{s\beta}{}^2 + e_{s\alpha}^2\right)}} \cdot \operatorname{sgn}(\omega_e) \tag{3.15}$$

$$\sin(\theta) = \frac{-e_{s\beta}}{\sqrt{\left(e_{s\beta}^2 + e_{s\alpha}^2\right)}} \cdot \operatorname{sgn}(\omega_e) \tag{3.16}$$

Here the definition of an error vector is discussed. The current error vector is defined as follows:

$$\varepsilon_{1(\alpha,\beta)} = \begin{bmatrix} \hat{i}_{s\alpha} \\ \hat{i}_{s\beta} \end{bmatrix} - \begin{bmatrix} i_{s\alpha} \\ i_{s\beta} \end{bmatrix} \tag{3.17}$$

and for the back-EMF, the error vector is:

$$\varepsilon_{2(\alpha,\beta)} = \begin{bmatrix} \hat{e}_{s\alpha} \\ \hat{e}_{s\beta} \end{bmatrix} - \begin{bmatrix} e_{s\alpha} \\ e_{s\beta} \end{bmatrix} \tag{3.18}$$

The sliding mode condition is set as below:

$$\varepsilon_{1(\alpha,\beta)} = \left\lfloor i_{s(\alpha,\beta)} - \hat{i}_{s(\alpha,\beta)} \right\rfloor = 0 \tag{3.19}$$

When the product of $\varepsilon_{l(\alpha,\beta)}$ and its derivative are below zero, the condition is satisfying and sliding mode occurs; the higher coefficient k_1 we have, the higher the possibility of occurring we get. Therefore the condition can be written as:

$$\varepsilon_{1(\alpha,\beta)} T \cdot \frac{d}{dt}\left(\varepsilon_{1(\alpha,\beta)}\right) < 0 \tag{3.20}$$

By Merging Equation 3.17 and Equation 3.18 with Equation 3.10 and Equation 3.9 error equation is calculated as follow:

$$\frac{d}{dt}\left[\varepsilon_{1(\alpha,\beta)}\right] = [A_{11} A_{12}] \cdot \begin{bmatrix} \varepsilon_{1(\alpha,\beta)} \\ \varepsilon_{2(\alpha,\beta)} \end{bmatrix} + k_1 \cdot I \cdot \operatorname{sgn}\left(\varepsilon_{1(\alpha,\beta)}\right) \tag{3.21}$$

3.1.2.1 Discrete time SMO in alpha-beta reference frame

Time discrete observer is achievable with the Euler-Arnold equation, which is shown in Equation 3.22 and Equation 3.23. The discrete-time observer is used in the Simulink part of this work, and it is used in digital control systems.

$$\begin{bmatrix} \hat{i}_{S(\alpha,\beta)} \\ \hat{e}_{S(\alpha,\beta)} \end{bmatrix}(k+1) = C \cdot K1 \cdot \begin{bmatrix} I \\ G \end{bmatrix} \cdot T_S \cdot \operatorname{sgn}\left(\hat{i}_{S(\alpha,\beta)}(k) - i_{S(\alpha,\beta)}(k)\right) \tag{3.22}$$

$$C = \left(I + \begin{bmatrix} A_{11} & A_{12} \\ 0 & A_{22} \end{bmatrix} \cdot T_S\right) \cdot \begin{bmatrix} \hat{i}_{S(\alpha,\beta)} \\ \hat{e}_{S(\alpha,\beta} \end{bmatrix}(k) + \begin{bmatrix} B_1 \\ 0 \end{bmatrix} \cdot T_S \cdot \left[u_{S(\alpha,\beta)}\right](k) \tag{3.23}$$

Equation 3.22 and Equation 3.23, which are the discrete-time model of sliding mode observer parameters, are described from Equation 3.24 to Equation 3.29.

$$\begin{bmatrix} A_{11} & A_{12} \\ 0 & A_{22} \end{bmatrix} \cdot T_S = \begin{bmatrix} -\frac{R_S}{L_S}T_S & 0 & -\frac{1}{L_S}T_S & 0 \\ 0 & -\frac{R_S}{L_S}T_S & 0 & -\frac{1}{L_S}T_S \\ 0 & 0 & 0 & -\omega_e T_S \\ 0 & 0 & \omega_e T_S & 0 \end{bmatrix} \tag{3.24}$$

$$B_1 \cdot T_S = \begin{bmatrix} \frac{1}{L_S}T_S & 0 \\ 0 & \frac{1}{L_S}T_S \end{bmatrix} \tag{3.25}$$

$$A_{11}T_S = a_{11}T_S \cdot I = -\frac{R_S}{L_S}T_S \cdot I \tag{3.26}$$

$$A_{12}T_S = a_{12}T_S \cdot I = -\frac{1}{L_S}T_S \cdot I \tag{3.27}$$

$$A_{22}T_S = \omega_e T_S \cdot J \tag{3.28}$$

$$B_1 T_S = b_1 T_S \cdot I = -a_{11}T_S \cdot I = \frac{1}{L_S}T_S \cdot I \tag{3.29}$$

3.1.2.2 SMO in d-q axis reference frame

The aforementioned d-q axis transformation (Chapter 2) has a key role in the rotating system due to its adaptive reference frame rotation. Thus, it benefits us to avoid over-calculation in salient machines in which the inductance in the d and q axis are not equal, and they vary significantly. For an ideal salient motor, these two inductances are constant. The back-EMF vector rotates with respect to the rotor angle; therefore, in the d-q axis reference frame coordination, its value is constant, and it only depends on the dynamics of the voltage and current [36, 37]. Block diagram of SMO control fed IPMSM is shown in Figure 3.2. From Equation 2.34 and Equation 2.35, state variables of IPMSM can be derived as following:

$$\frac{d}{dt}\begin{bmatrix} i_{sd} \\ i_{sq} \\ e_{sd} \\ e_{sa} \end{bmatrix} = \begin{bmatrix} -\frac{R_s}{L_{sd}} & \omega_e \frac{L_{sq}}{L_{sd}} & -\frac{1}{L_{sd}} & 0 \\ \omega_e \frac{L_{sd}}{L_{sq}} & -\frac{R_s}{L_{sq}} & 0 & -\frac{1}{L_{sq}} \\ 0 & 0 & 0 & 0 \\ 0 & 0 & 0 & 0 \end{bmatrix} \cdot \begin{bmatrix} i_{sd} \\ i_{sq} \\ e_{sd} \\ e_{sq} \end{bmatrix} + \begin{bmatrix} \frac{1}{L_{sd}} & 0 \\ 0 & \frac{1}{L_{sq}} \\ 0 & 0 \\ 0 & 0 \end{bmatrix} \cdot \begin{bmatrix} u_{sd} \\ u_{sq} \end{bmatrix} \tag{3.30}$$

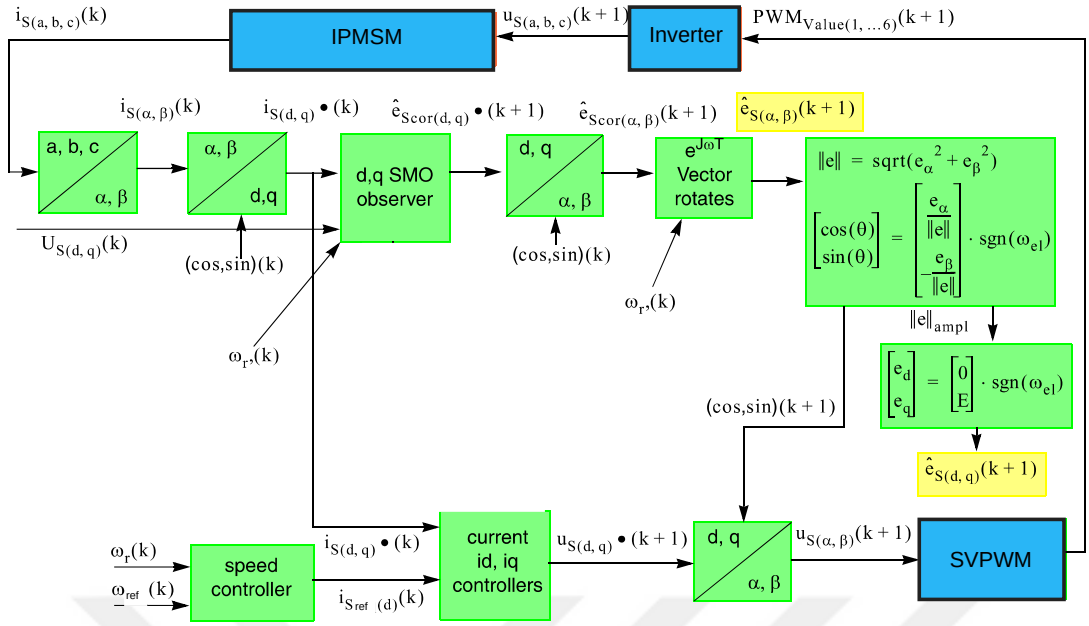

Figure 3.2 : Block diagram of SMO control fed IPMSM.

Equation 3.30 can be simplified as follow:

$$\frac{d}{dt}\begin{bmatrix} i_{sd} \\ i_{sq} \\ e_{sd} \\ e_{sq} \end{bmatrix} = \begin{bmatrix} a_{11} & a_{12} & a_{13} & 0 \\ a_{21} & a_{22} & 0 & a_{24} \\ 0 & 0 & 0 & 0 \\ 0 & 0 & 0 & 0 \end{bmatrix} \cdot \begin{bmatrix} i_{sd} \\ i_{sq} \\ e_{sd} \\ e_{sq} \end{bmatrix} + \begin{bmatrix} b_{11} & 0 \\ 0 & b_{22} \\ 0 & 0 \\ 0 & 0 \end{bmatrix} \cdot \begin{bmatrix} u_{sd} \\ u_{sq} \end{bmatrix} \tag{3.31}$$

$$\frac{d}{dt}\begin{bmatrix} \hat{i}_{s(d,q)} \\ \hat{e}_{s(d,q)} \end{bmatrix}(t) = K_c + K_l \cdot \begin{bmatrix} I \\ G \end{bmatrix} \cdot \operatorname{sgn}\left(\hat{i}_{s(d,q)}(t) - i_{s(d,q)}(t)\right) \tag{3.32}$$

and K_c equals:

$$K_c = \begin{bmatrix} a_{I1} & a_{12} & a_{13} & 0 \\ a_{21} & a_{22} & 0 & a_{24} \\ 0 & 0 & 0 & 0 \\ 0 & 0 & 0 & 0 \end{bmatrix} \cdot \begin{bmatrix} \hat{i}_{s(d,q)} \\ \hat{e}_{s(d,q)} \end{bmatrix}(t) + \begin{bmatrix} b_{11} & 0 \\ 0 & b_{22} \\ 0 & 0 \\ 0 & 0 \end{bmatrix} \cdot \left[u_{S(d,q)}\right](t) \tag{3.33}$$

The estimated position of the rotor is obtained by calculating the inverse tangent of the estimated BEMF of α over the estimated BEMF of β in the $\alpha - \beta$ reference frame [37]. The representative equation is shown in Equation 3.34.

$$\hat{\theta} = \tan^{-1}\left(-\frac{\hat{e}_{S\alpha}}{\hat{e}_{S\beta}}\right) \tag{3.34}$$

4. NOTCH FILTER IN CONTROL SYSTEMS

Filters play the main role in control systems by reducing noise and unwanted resonances which disturb the feedback in the system. Mostly filters are employed by communication engineers to reduce the distortion; here, we use these filters from a control engineering perspective to attenuate the effect of redundant signals in the feedback and estimation [38]. Low-pass filters are the most common ones in this field and are used to eliminate the intrinsic noise in the feedback of IPMSM, which is generated due to the inevitable subtle asymmetric structure of the motor. The main disadvantage of a low-pass filter is the instability which occurs because of phase lag at specific frequencies such as gain crossover frequency. Notch filters, thanks to their design, are less limited in those applications; [39] both advantageous and disadvantageous for this filter are less intense than low-pass filters [40]. In this chapter, an overview is revolved around the notch filter, and it is explained more, then mathematical equations of this filter are represented and discussed.

4.1 Notch Filter

A notch filter is a second-order filter with two zeros and two poles where poles are lightly damped.

The transfer function for the notch filter is shown in Equation 4.1

$$H(z) = K\frac{\left(z - e^{+j\omega_n}\right)\left(z - e^{-j\omega_n}\right)}{\left(z - ae^{+j\omega_n}\right)\left(z - ae^{-j\omega_n}\right)} \tag{4.1}$$

Equation 4.1 can be written as follows: Equation 4.2.

$$H(z) = K\frac{z^2 - 2z\cos\omega_n + 1}{\left(z^2 - 2az\cos\omega_n + a^2\right)} \tag{4.2}$$

Where ω_n is the notch frequency and if $z = -1$, K is determined as:

$$K = \frac{1 + 2a\cos\left(\omega_n\right) + a^2}{2 + 2\cos\left(\omega_n\right)} \tag{4.3}$$

Table 4.1 : Parameters of the designed notch filter

Parameter's name	value
Filter order	6
Center frequency	0.5
Quality factor	10
Passband ripple	1

ω_n can be defined with input frequency oversampling frequency. See Equation 4.4.

$$\omega_n = \frac{f_c}{f_s} \tag{4.4}$$

For the ideal notch filter, the gain at notch frequency is zero. When s=jwl,thus s=wn and causes the Equation 4.1 to be zero (-∞ dB)

A notch filter is a bi-quad filter where wn = wd and en = 0; therefore, by configuring those two parameters notch filter is applicable to the system. The equation for bi-quad (bi-linear quadratic), which is named because of two quadratic terms [41], is shown in Equation 4.1.

Frequency response of the notch filte, phase response of the notch filter ,and Zero-pole plot of the notch filter are shown in Figure 4.1, Figure 4.2, and Figure 4.3 respectively.

The damping ratio, ζ, in the notch filter is usually set below 1.0; in order to get a sharper filter, ζ should be set in lower values; hence the lower the ζ, the sharper gain. In order to attenuate the desired signal thoroughly, a precise choice of coefficients is required. High ζ causes the filter to concentrate more at the center.

Here are the parameters for designing a notch filter; see table 4.1

As is shown in Figure 4.3, when designing a notch filter, it is needed to place poles close to the zeros in order to create a deep and narrow notch. The placement of poles and zeros determines the shape and characteristics of the frequency response of the filter. By putting poles close to the zeros, the transfer function of the filter will exhibit a deep and narrow notch in the frequency domain [42].

As we know, zeros are points in the transfer function where the response is zero, while poles are points where the response approaches infinity. By placing poles near zeros, the response of the filter at those frequencies is significantly attenuated, resulting in the creation of a notch.

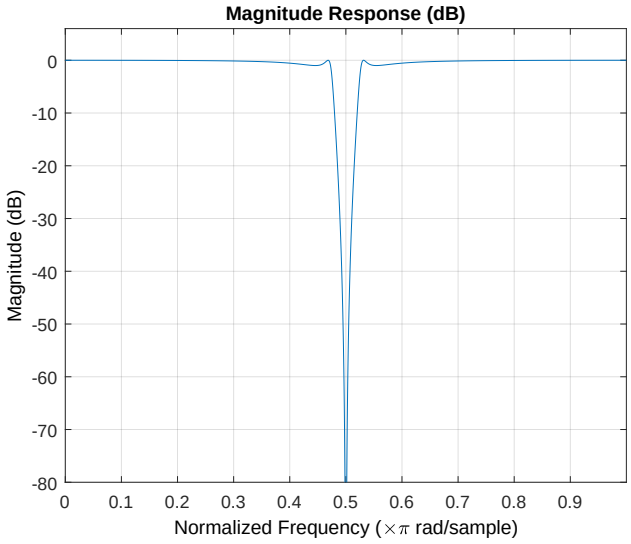

Figure 4.1 : Frequency response of the notch filter

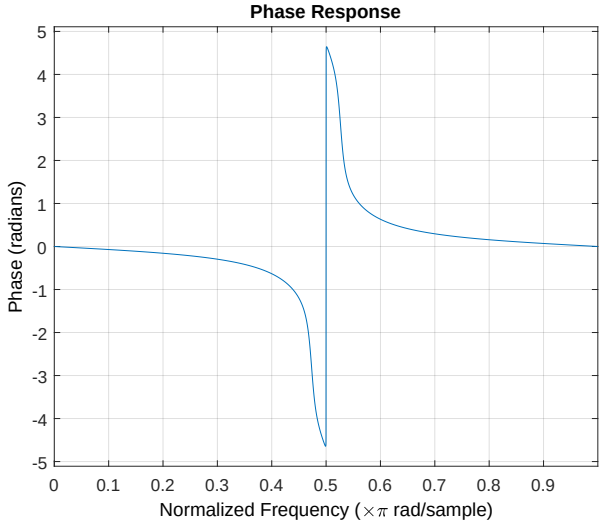

Figure 4.2 : Phase response of the notch filter with parameters shown in table 4.1

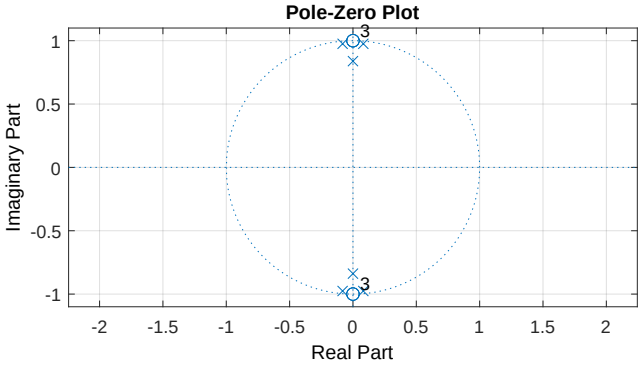

Figure 4.3 : Zero-pole plot of the notch filter with parameters shown in table 4.1

The close proximity of poles to zeros allows for a more precise and effective cancellation of specific frequencies. The notch becomes narrower because the poles and zeros

interact in such a way that they cancel each other's effects more strongly at the desired frequency see Figure 4.1. This configuration enables the filter to provide a high level of attenuation within a narrow frequency range while having minimal impact on the frequencies outside the notch, therefore placing poles close to zeros in a notch filter design allows for a deep and narrow attenuation of a specific frequency range, enabling effective rejection of unwanted signals [43].

4.2 Variable Notch Filter

A variable notch filter is a type of filter used in control systems to attenuate specific frequency components of a signal. It is called a "notch" filter because it creates a "notch" or a deep narrow dip in the frequency response curve of the filter at the specific frequency to be attenuated.

The term "variable" refers to the fact that the center frequency of the notch is adjustable or tuned based on the specific application requirements, which is accomplished by changing the values of the filter's coefficients.

In control systems, a notch filter is often used to attenuate unwanted oscillations or resonances in the system [44]. For example, in a motor control system, a variable notch filter is used to attenuate the resonant frequency of the motor, which can cause instability and oscillations in the system. By attenuating the resonant frequency, the filter helps to stabilize the system and improve its performance.

Variable notch filter has an adjustable feature and lets us benefit from its frequency filtering properties in a wider range. Therefore, it plays a main role in reaching the purpose of error reduction in sliding mode observer control for different speed ranges. In Figure 4.4, input and output are defined as U and Y, respectively, Parameters a, b, c, d, which are tags from a sub-block shown in Figure 4.5.

4.3 Utilizing Variable Notch Filter in SMO

In sliding mode observer control, a variable notch filter can be used to improve the observer's estimation accuracy and robustness to measurement noise and disturbances. Variable notch filters can be merged and used in combination with a sliding mode observer, which is a nonlinear observer that estimates the state of a system by minimizing

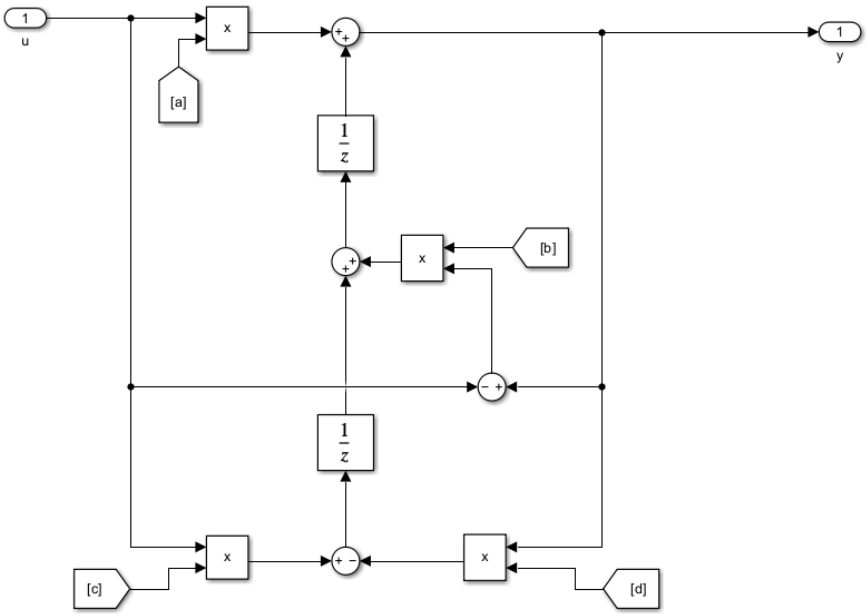

Figure 4.4 : Block diagram of variable notch filter-(1).

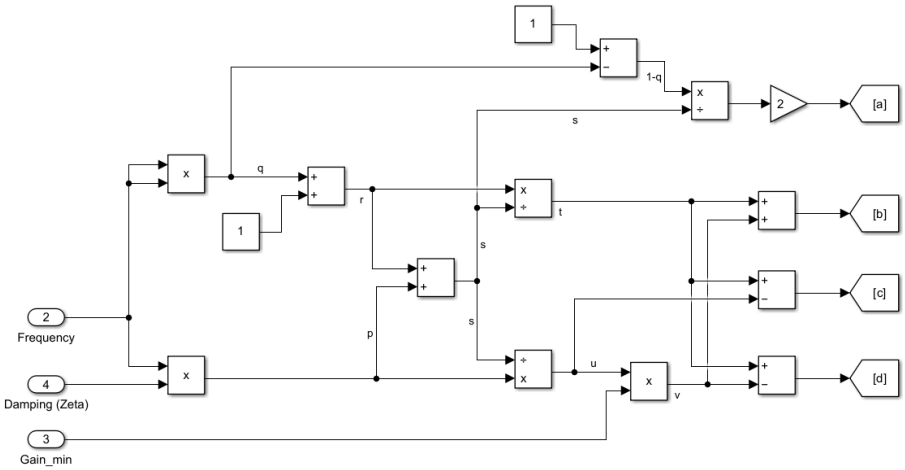

Figure 4.5 : Block diagram of variable notch filter-(2).

the sliding mode function. Due to this reason, oscillation in the estimation output of SMO is happening, and this oscillation is a function of the rotor frequency or, in other words, a function of the desired speed. Frequency response of notch filter simulated in MATLAB®/Simulink® is shown in Figure 4.6.

To use a variable notch filter in sliding mode observer control, these steps should be followed:

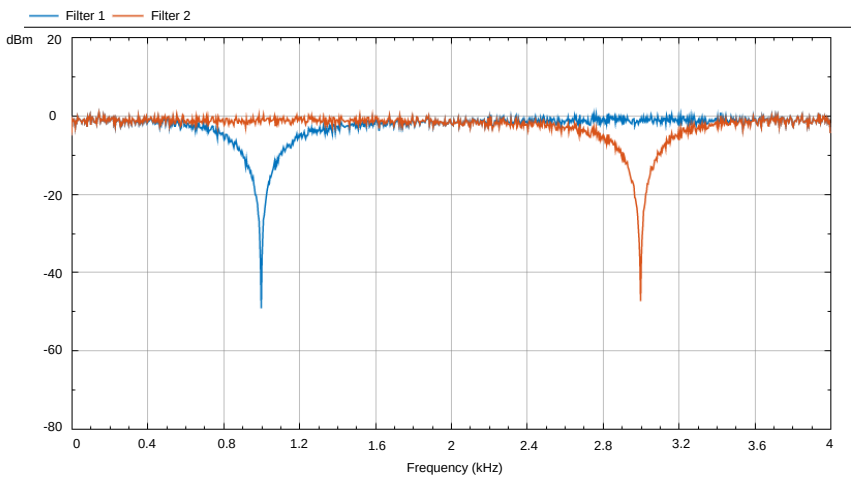

Figure 4.6 : Frequency response of notch filter simulated in MATLAB®/Simulink®.

Identifying the frequency component which is required to be attenuated. In this case, that frequency is calculated by the rotor's rotation frequency, that is affecting the observer's estimation accuracy.

Then, Once the frequency component is identified, designing the variable notch filter is needed to attenuate that frequency. The filter can be designed using standard filter design techniques, such as the Butterworth or Chebyshev filters. The filter parameters, such as the notch frequency and the filter order, are adjusted based on the fluctuation rate and intensity.

In this case, the variable notch filter is designed in MMATLAB®/Simulink® and the represented block diagram is shown in Figures 4.4 and 4.5.

After implementing the filter, the output signal is used as an estimated feedback signal with less error. A comparison of the error reduction in different speed ranges is presented in Chapter 5; therefore, we can see that combining a variable notch filter with a sliding mode observer improves the estimation accuracy and robustness.

By using a variable notch filter in sliding mode observer control, the observer's estimation accuracy is enhanced, and the robustness of the system, thanks to a less estimated error, is increased. This can lead to better control system performance and stability.

5. SIMULATION

The simulation consists of three main parts: Inverter and IPMSM, current control block and speed control block, where in this thesis, the main focus is on sliding mode observer and variable notch filter in the current control block. The block diagram of the main section is shown in Figure 5.2.

IPMSM parameters chosen in this Simulink are shown in the table 5.1

A feed-forward from speed reference is employed to adjust the notch filter coefficient and frequency.

The speed control block is expanded and shown in Figure 5.1 Reference speed is converted to the per-unit system, and for conversion from rpm to per-unit, the gain is set to "1/N_base" where the value for N_base is shown in Table 5.1.

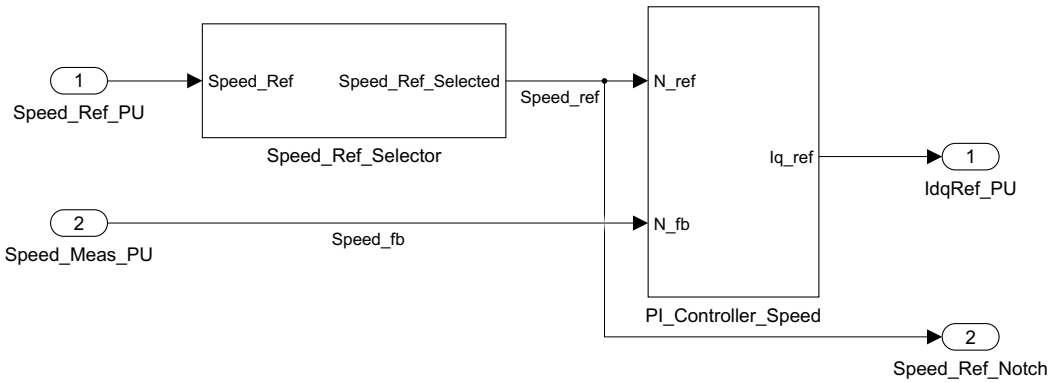

Figure 5.1 : Block-diagram of speed control.

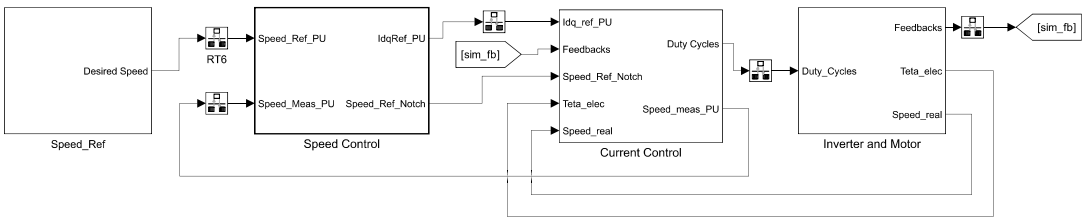

Figure 5.2 : Block-diagram of the proposed method in MATLAB®/Simulink®.

Table 5.1 : IPMSM parameters

Parameter	value
poles	4
Stator resistance	0.36
Ld	3.752e-4
Lq	4.148e-4
J	7.0616e-06
B	2.6369e-06
Ke	4.6400
Kt	0.0384
I_rated	7.1000
N_base	4107

Speed_Ref_Selector changes the speed reference from open-loop to close-loop when the simulation is running at "T_Ref_openLoop" which is equal to T=1s.

In the speed control block, a PI controller is used to adjust the current of the motor to achieve the desired speed. See Figure 5.3.

The PI controller provides speed control by regulating the motor's current accurately to keep the speed constant. It compares the actual speed with the desired speed and adjusts the current of the motor to maintain the motor's speed close to the desired reference speed. PI controllers are robust and reliable. They are able to handle various disturbances, such as changes in the load or voltage fluctuations, and they only require two parameters, the proportional gain and the integral gain, to be set. These gains are tuned to achieve an acceptable response. In this case, the proportional parameter for the speed control loop, K_p is set to 0.4595, and the integral parameter K_I is set to 0.0061.

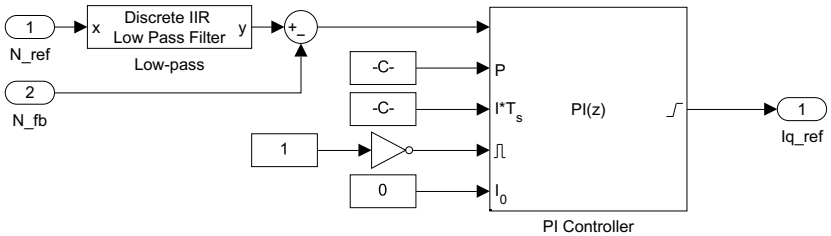

Figure 5.3 : Schematic of PI controller.

A low pass filter with a coefficient of 0.2 is applied before the PI controller for zero cancellation. The estimated speed is deducted from the desired speed as it is shown in Figure 5.3.

After estimating and calculating the speed and position of IPMSM with the conventional sliding mode observer control, the proposed method by using a variable notch filter, is applied to the system. As it is shown in Figure 5.4, a low pass filter and a DC component removal block is employed before any modification by the notch filter. Sub-block of DC component removal is shown in Figure 5.5 where the low-pass coefficient for this block is set to 0.005 or more precisely (0.005*(T_s/50e-6))

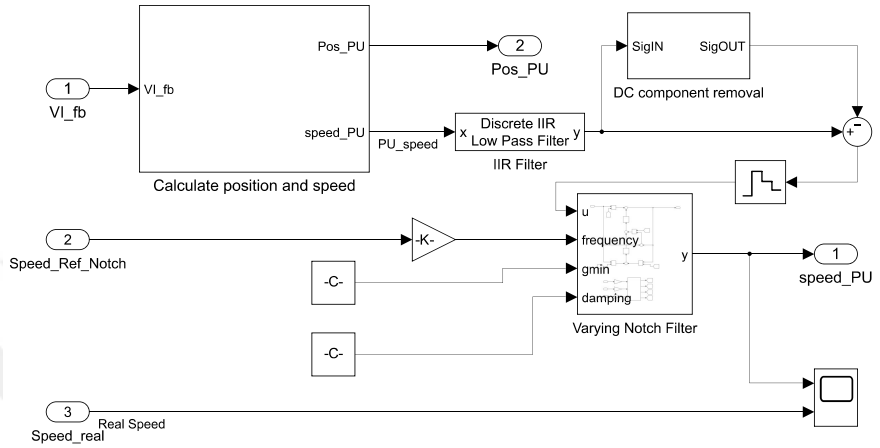

Figure 5.4 : Speed and position estimation with the presence of proposed varying notch filter block.

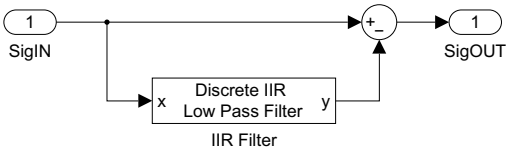

Figure 5.5 : DC component removal block

As it is explained in Chapter 3, in sensorless control of an IPMSM, a sliding mode observer (SMO) is used to estimate the rotor position and speed without the use of a physical sensor. However, the SMO can be sensitive to high-frequency noise, which can degrade the accuracy of the estimated position and speed. Fluctuations in the estimated speed, see Figure 5.13, is inevitable in the SMO control; therefore, a notch filter is used in the SMO to reduce the impact of high-frequency noise and reference speed alternation on the estimated position and speed.

Block diagram for sliding mode observer in MATLAB®/Simulink® is shown in Figure5.6 and consists of four inputs V_α, V_β, i_α, and i_β which are calculated by Clarke transformation block, (Clarke transformation is explained in Chapter 2). $\hat{e}_{s(\alpha)}$ and $\hat{e}_{s(\beta)}$ are calculated from "e_alpha_estimator" and "e_beta_estimator" blocks. Close-loop block is presented in Figure 5.7.

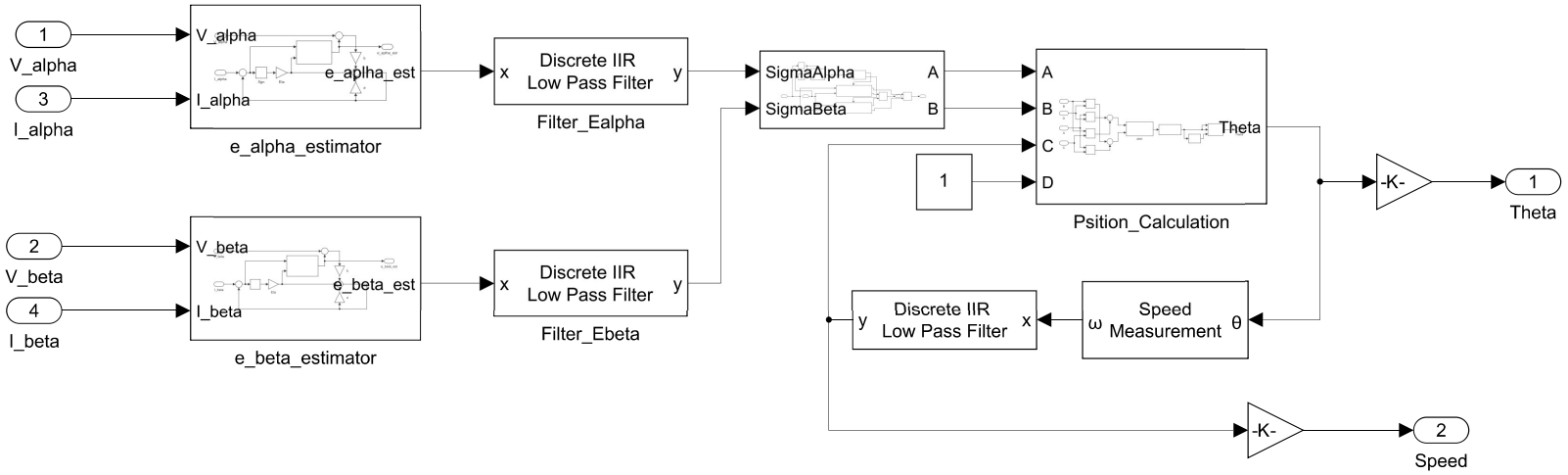

Figure 5.6 : Block diagram of sliding mode observer.

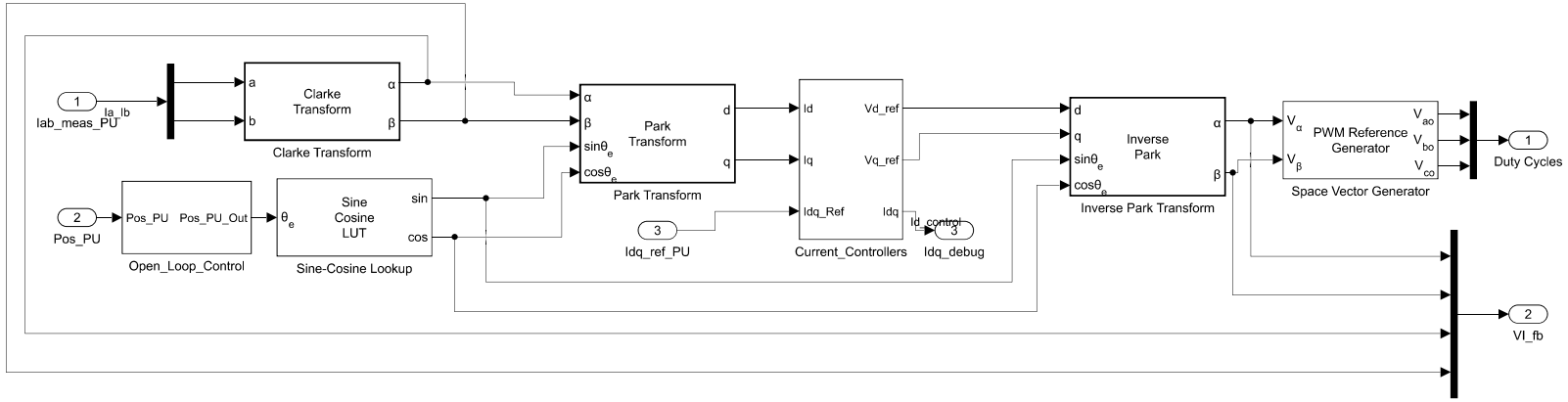

Figure 5.7 : Close-loop block of the simulation.

e_alpha_estimator block is shown in Figure 5.8. A sign function is applied to i_α and then multiplied by the current observer gain to get η, then η is connected to the Zk port of disturbance observer. The subsystem is shown in Figure 5.9. In Figure 5.9, gain "a" is set to (exp(StatorResistance×BlkSampleTime(1)/StatorInductance)) and after adding ζ and i_alpha_err to it, gain "b" which is (Disturbance Observer Gain/((1-exp(-Stator Resistance×BlkSampleTime(1)/StatorInductance))/Stator Resistance)) is applied to the system.

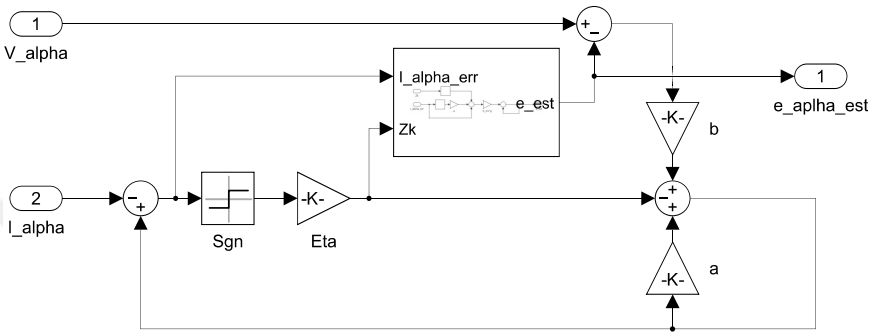

Figure 5.8 : e_α estimator.

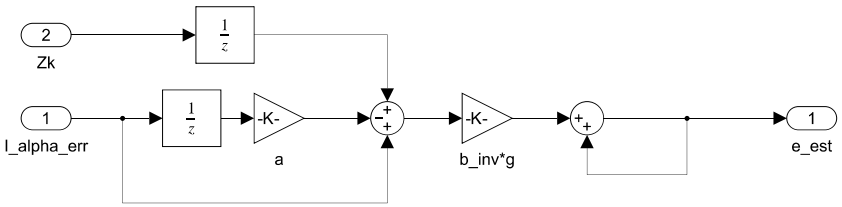

Figure 5.9 : Disturbance observer subsystem.

Block "subsystem 5" is used to latch the direction. First, sensing the direction of the signal is needed, which is shown as the "Direction_Sensing" block in Figure 5.10. "Direction_Sensing" is shown in Figure 5.11 where there is a switch, either zero or one, in this block.

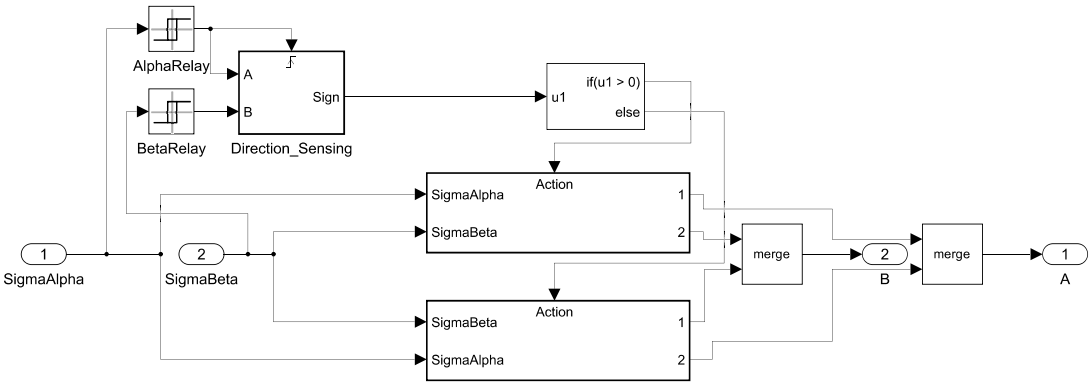

Figure 5.10 : Direction latch block

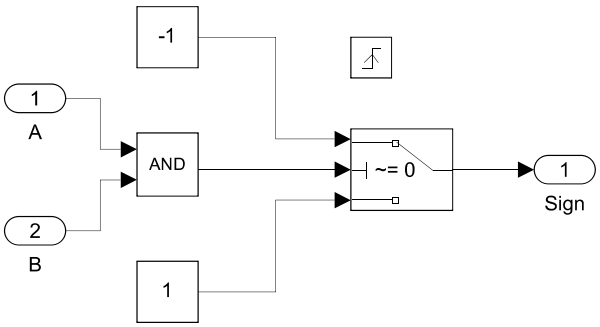

Figure 5.11 : Direction sensing block.

The last part for getting the estimated position is the position estimation block which consists of four inputs (A, B, C, and D) where A and B are got from the latching direction, and D has the constant "CutoffFreq/(MaxApplicationSpeed×PolePairs/60)", and C is a feedback loop from the estimated speed. See Figure 5.12.

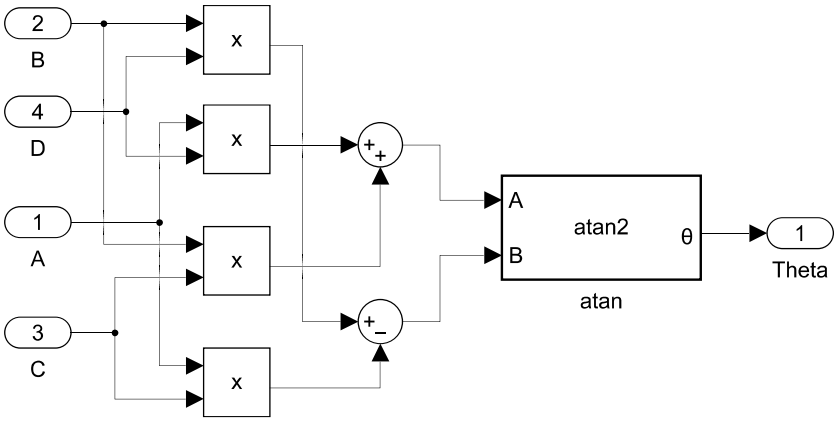

Figure 5.12 : Position calculation scheme.

After getting the estimated back emf from α and β parameters in the stationary orthogonal frame, it is possible to reach the position of the motor from the obtained data from the block in Figure 5.8. To eliminate high-frequency noises, a low pass filter with (2×π×Cutoff Frequency×T_s/(2×π×Cutoff Frequency×T_s+1)) coefficient is employed before the position estimation block.

Fluctuation, originating from the sign function, occurs in the estimator, and the sign function block is placed before the input of the disturbance observer block in Figure5.8. Fluctuation for the speed 0.1 pu and 0.2 pu is shown in Figure 5.13 and Figure 5.14, respectively.

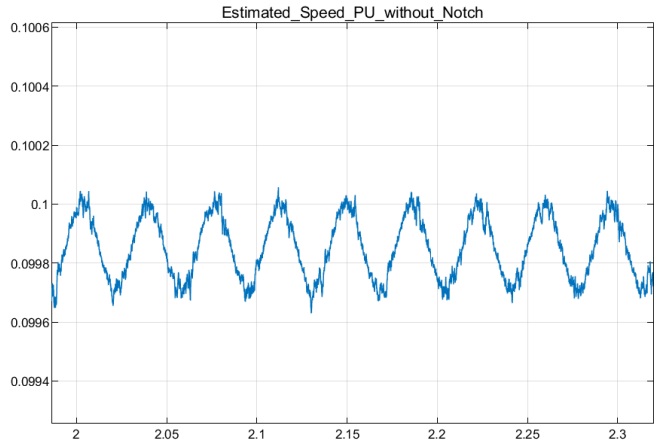

Figure 5.13 : Speed estimation fluctuation in 0.1 pu.

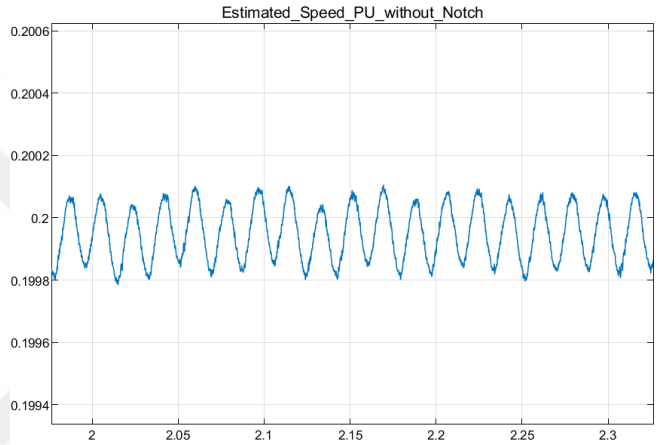

Figure 5.14 : Speed estimation fluctuation in 0.2 pu.

From Figure 5.13 and Figure 5.14, it can be deduced that the fluctuation frequency is not the same in different speed ranges. Thus a constant notch filter cannot be an efficient choice for error mitigation.

After sensing the direction of the sliding in subsystem 5, which is shown in Figure5.6, the position of the rotor is calculated from the Equation 3.34 and it is shown in Figure5.12

As it is shown in Figure 5.15, the position error is decreased. Estimated error fluctuates from zero to 4×10^{-4} in the per-unit system, and after applying the notch filter, it is diminished and fluctuates from zero to 1×10^{-4}.

After the FFT analysis of the position estimation signal, a significant reduction of the magnitude of the oscillated frequency is detected, and it is reduced from 0.14 to 0.06. Figure 5.16 and Figure 5.17 show the FFT analysis before and after applying the notch filter, respectively.

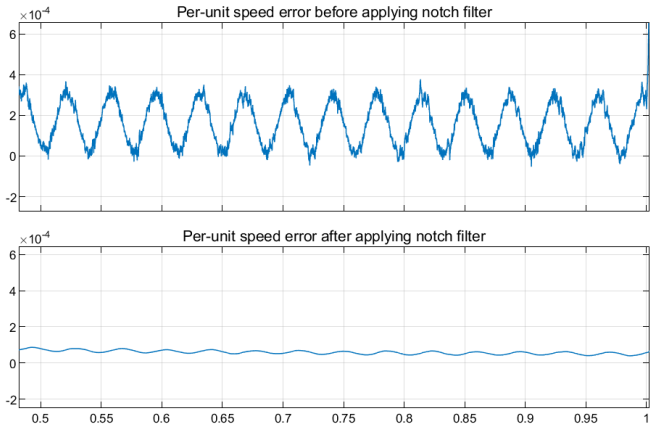

Figure 5.15 : Position error reduction before and after applying notch filter

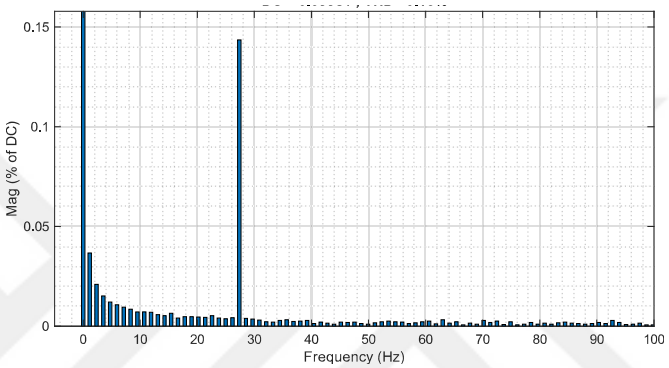

Figure 5.16 : FFT analysis before applying notch filter in 0.1 p.u reference speed.

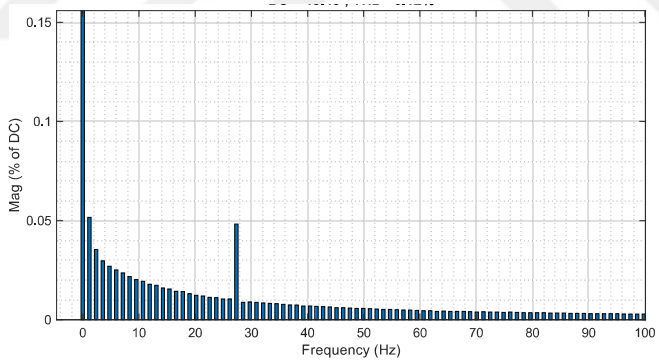

Figure 5.17 : FFT analysis after applying notch filter in 0.1 p.u reference speed.

In Figure 5.19, which shows the FFT analysis of estimated speed when the reference speed is 0.5 pu, it can be seen that there are two major frequencies or, let's say, oscillations. One is around 13 Hz, and the other one is 137 Hz. For eliminating those two frequencies, the double-notch filter is recommended, which hasn't been investigated in the current study. Double or multiple-notch filters can be investigated in future works. By applying only one notch filter whose configuration is set for 13 Hz, the amplitude of the aforementioned frequency decreases from 6.5×10^{-3} to 4.6×10^{-3}.

In contrast, attenuating the higher frequency (137 Hz) has some advantages. Amplitude of the error decreases from 6×10^{-3} to 1.4×10^{-3}

You can see the estimated error signal before and after applying the notch filter to 137 Hz frequency in Figure 5.18 when the motor is rotating in 0.5 p.u.

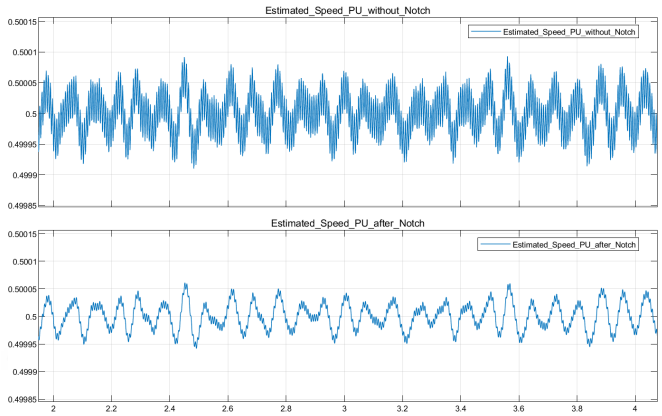

Figure 5.18 : Estimated signal after and before applying notch filter in 0.5 p.u reference speed.

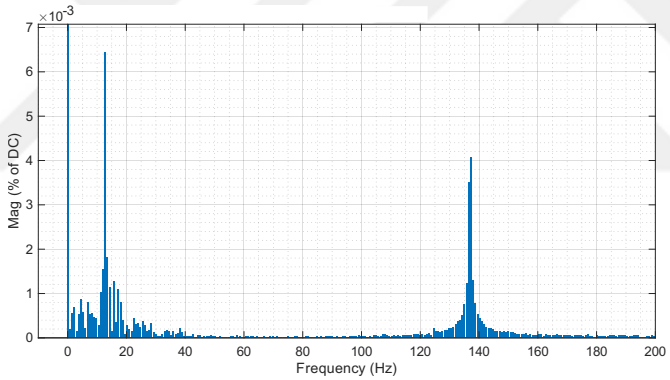

Figure 5.19 : FFT analysis before applying notch filter in 0.5 p.u reference speed.

As it is shown in Figure 5.20, after applying the proposed method to high-frequency rotor rotation, where in this case the speed is 0.5 pu,

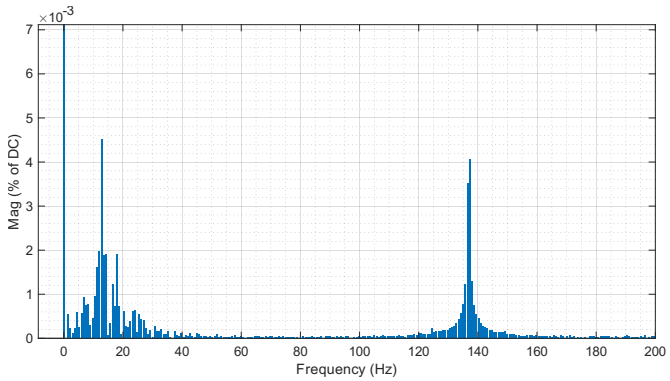

Figure 5.20 : FFT analysis after applying notch filter in 0.5 pu reference speed.

FFT analysis of estimated speed signal after and before applying 137 Hz notch filter in Figure 5.21 and Figure 5.22 shows that the amplitude of high frequency (137 Hz) decreased from 5.9×10^{-3} to 1.4×10^{-3}

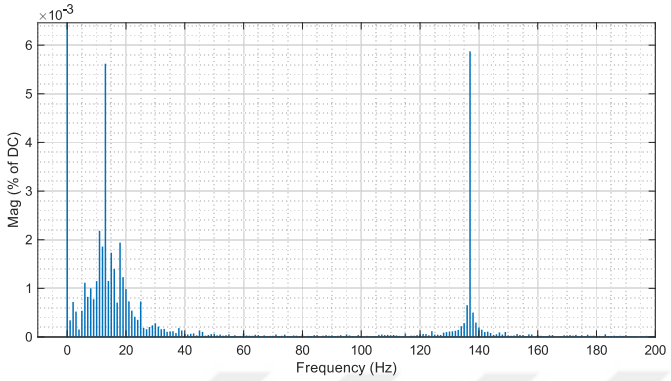

Figure 5.21 : FFT analysis before applying notch filter in 0.5 pu reference speed to 137 Hz.

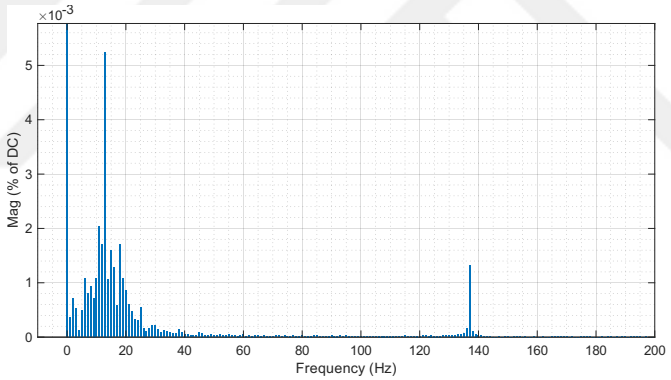

Figure 5.22 : FFT analysis after applying notch filter in 0.5 pu reference speed to 137 Hz.

Here are the key roles of a notch filter in SMO for sensorless control:

Filtering high-frequency noise: A notch filter is designed to attenuate a specific frequency or range of frequencies. It can be used to filter out high-frequency noise that can affect the accuracy of the estimated rotor position and speed.

Improving robustness: By filtering out high-frequency noise, the notch filter can improve the robustness of the SMO to noise and disturbances. This can result in more accurate and stable estimates of the rotor position and speed, which are crucial for the proper operation of a PMSM.

Enhancing the convergence rate: A well-designed notch filter can enhance the convergence rate of the SMO, allowing it to estimate the rotor position and speed more quickly and accurately. This can improve the overall performance of the sensorless control system, making it more responsive and efficient.

Overall, the notch filter plays an important role in the sensorless control of a PMSM with an SMO. By filtering out high-frequency noise and improving the robustness and convergence rate of the SMO, the notch filter can help ensure the accurate and stable operation of the motor.

5.1 Simulation Results

According to the results getting from the MATLAB®/Simulink®, chattering in the SMO control model which increases the error oscillation in the system is reduced to 1×10^{-4} in amount, for instance as it is shown in Figure 5.15 significant reduction from 4×10^{-4} to 1×10^{-4} of speed estimation in per unit is observed. therefore a variable notch filter is a solution for oscillation mitigation to increase the estimation accuracy in order to gain higher robustness and efficiency.

As it is shown in Figure 5.16 and Figure 5.17, the magnitude of the first harmonic of the chattering frequency in 0.1 per unit decreased from 0.14 to 0.05, so that less error in the estimated speed is desirable.

6. FUTURE WORK AND RECOMMENDATIONS

As is explained in Chapter 5, in the higher speed, for example, 0.5 pu, there are two main harmonics in the speed estimation signal's frequency response, therefore both should be eliminated to reduce chattering in the SMO method. Double notching can be the next generation of this study, being able to eliminate all unwanted frequencies in any speed range.

REFERENCES

[1] **Montesinos, D.**, **Galceran, S.**, **Sudria, A.**, **Gomis, O. and Blaabjerg, F.** (2005). Low cost sensorless control of permanent magnet motors - an overview and evaluation, *IEEE International Conference on Electric Machines and Drives, 2005.*, pp.1681–1688.

[2] **Woldegiorgis, A.T.**, **Ge, X.**, **Wang, H. and Hassan, M.** (2021). A New Frequency Adaptive Second-Order Disturbance Observer for Sensorless Vector Control of Interior Permanent Magnet Synchronous Motor, *IEEE Transactions on Industrial Electronics*, *68*(12), 11847–11857.

[3] **Wang, Y.**, **Feng, Y.**, **Zhang, X. and Liang, J.** (2020). A New Reaching Law for Antidisturbance Sliding-Mode Control of PMSM Speed Regulation System, *IEEE Transactions on Power Electronics*, *35*(4), 4117–4126.

[4] **Doan, Q.V.**, **Vo, A.T.**, **Le, T.D.**, **Kang, H.J. and Nguyen, N.H.A.** (2020). A Novel Fast Terminal Sliding Mode Tracking Control Methodology for Robot Manipulators, *Applied Sciences*, *10*(9).

[5] **Wen, D.**, **Wang, W. and Zhang, Y.** (2022). Sensorless Control of Permanent Magnet Synchronous Motor in Full Speed Range, *Chinese Journal of Electrical Engineering*, *8*(2), 97–107.

[6] **Xin, L. and Bin, Z.** (2018). Sensorless Adaptive Sliding Mode FCS–MPC Using Extended State Observer for PMSM Systerm, *2018 IEEE International Conference of Intelligent Robotic and Control Engineering (IRCE)*, pp.171–177.

[7] **Filho, C.J.V.**, **Xiao, D.**, **Vieira, R.P. and Emadi, A.** (2021). Observers for High-Speed Sensorless PMSM Drives: Design Methods, Tuning Challenges and Future Trends, *IEEE Access*, *9*, 56397–56415.

[8] **Wang, G.**, **Li, T.**, **Zhang, G.**, **Gui, X. and Xu, D.** (2014). Position Estimation Error Reduction Using Recursive-Least-Square Adaptive Filter for Model-Based Sensorless Interior Permanent-Magnet Synchronous Motor Drives, *IEEE Transactions on Industrial Electronics*, *61*(9), 5115–5125.

[9] **Wang, G.**, **Zhan, H.**, **Zhang, G.**, **Gui, X. and Xu, D.** (2014). Adaptive Compensation Method of Position Estimation Harmonic Error for EMF-Based Observer in Sensorless IPMSM Drives, *IEEE Transactions on Power Electronics*, *29*(6), 3055–3064.

[10] **Karimi-Ghartemani, M.**, **Khajehoddin, S.A.**, **Jain, P.K.**, **Bakhshai, A. and Mojiri, M.** (2012). Addressing DC Component in PLL and Notch Filter Algorithms, *IEEE Transactions on Power Electronics*, *27*(1), 78–86.

[11] **Ciobotaru, M.**, **Teodorescu, R. and Agelidis, V.G.** (2008). Offset rejection for PLL based synchronization in grid-connected converters, *2008 Twenty-Third Annual IEEE Applied Power Electronics Conference and Exposition*, pp.1611–1617.

[12] **Karimi-Ghartemani, M. and Iravani, M.** (2003). Wide-range, fast and robust estimation of power system frequency, *Electric Power Systems Research*, *65*(2), 109–117.

[13] **Tian, L.**, **Liu, Y.**, **Zhao, J. and Sun, J.** (2015). The sensorless control of IPMSM based on improved sliding-mode observer, *The 27th Chinese Control and Decision Conference (2015 CCDC)*, pp.935–940.

[14] **Zhao, Y.**, **Qiao, W. and Wu, L.** (2012). Position extraction from a discrete sliding-mode observer for sensorless control of IPMSMs, *2012 IEEE International Symposium on Industrial Electronics*, pp.725–730.

[15] **Tang, Q.**, **Chen, B.**, **He, X. and Shen, A.** (2019). Sensorless IPMSM Control Based on Improved Sliding Mode Observer by Using Synchronous Reference Frame Filter, *2019 20th Workshop on Control and Modeling for Power Electronics (COMPEL)*, pp.1–5.

[16] **Inoue, M. and Doki, S.** (2018). PMSM Model Discretization in Consideration of Park Transformation for Current Control System, *2018 International Power Electronics Conference (IPEC-Niigata 2018 -ECCE Asia)*, pp.1228–1233.

[17] **Pang, D.C.**, **Shi, Z.J.**, **Chang, Y.H.**, **Huang, H.C. and Bui, G.T.** (2021). Investigation of an Interior Micro Permanent Magnet Synchronous Motor, *Energies*, *14*(14).

[18] **AKYÜN, Y.**, **NORY, H.**, **TALAS, M.Z. and KÜRÜM, H.** (2019). Design Analysis and Verification of PMSM Motor For Dishwasher Machine, *2019 4th International Conference on Power Electronics and their Applications (ICPEA)*, pp.1–7.

[19] **Chen, B.**, **Wu, J.**, **Sun, Q.**, **Wu, H. and Zhang, L.** (2019). FEA-Based Mathematical Modeling and Simulation for IPMSM Drive with Consideration of Saturation and Cross-Coupling Influence, *2019 22nd International Conference on Electrical Machines and Systems (ICEMS)*, pp.1–5.

[20] **Di Tommaso, A.O.**, **Miceli, R.**, **Nevoloso, C.**, **Scaglione, G. and Schettino, G.** (2022). Improved High-Fidelity IPMSM mathematical model Including Saturation, Cross-Coupling, Torque Ripple and Iron Loss effects, *2022 International Conference on Electrical Machines (ICEM)*, pp.21–27.

[21] **Thike, R. and Pillay, P.** (2020). Mathematical Model of an Interior PMSM With Aligned Magnet and Reluctance Torques, *IEEE Transactions on Transportation Electrification*, *6*(2), 647–658.

[22] **Amornwongpeeti, S.**, **Kiselychnyk, O.**, **Wang, J.**, **Shatti, N.**, **Shah, N. and Soumelidis, M.** (2017). Adaptive torque control of IPMSM motor drives for electric vehicles, *2017 IEEE 26th International Symposium on Industrial Electronics (ISIE)*, pp.226–231.

[23] **Shen, H. and Zhang, C.** (2017). A new efficient sensorless I/f control method for IPMSM drives, *2017 IEEE 26th International Symposium on Industrial Electronics (ISIE)*, pp.209–213.

[24] **Wang, S.**, **Kang, J.**, **Degano, M.**, **Galassini, A. and Gerada, C.** (2020). An Accurate Wide-Speed Range Control Method of IPMSM Considering Resistive Voltage Drop and Magnetic Saturation, *IEEE Transactions on Industrial Electronics*, *67*(4), 2630–2641.

[25] **Muazzam, H.**, **Ishak, M.K.**, **Hanif, A.**, **Bhatti, A.**, **Isa, N.A.M. and Mahyuddin, M.N.** (2022). Vector Control of IPMSM used in Electric Vehicles, *2022 13th Asian Control Conference (ASCC)*, pp.1317–1321.

[26] **Won, I.K.**, **Kim, D.Y.**, **Jang, Y.H.**, **Choo, K.M.**, **Hong, S.W. and Won, C.Y.** (2016). Improved FOC of IPMSM using model predictive current control decreasing switching loss for EV, *2016 19th International Conference on Electrical Machines and Systems (ICEMS)*, pp.1–6.

[27] **Ludwig, F. and Möckel, H.A.** (2014). A dynamic angle calibration method for sensored FOC-controlled IPMSM in field weakening region, *2014 International Symposium on Power Electronics, Electrical Drives, Automation and Motion*, pp.825–829.

[28] **Ejlali, A.**, **Khaburi, D.A. and Soleimani, J.** (2016). Application of multiband hysteresis modulation in field oriented control based IPMSM drive fed by asymetrical multilevel cascaded H-Bridge inverter, *2016 7th Power Electronics and Drive Systems Technologies Conference (PEDSTC)*, pp.48–52.

[29] **Ahmed, T.**, **Das, A. and Halder, K.K.** (2014). Comparison of DTC and FOC for FSTP inverter fed IPMSM drives, *2013 International Conference on Electrical Information and Communication Technology (EICT)*, pp.1–5.

[30] **Tang, Y.**, **Xu, W.**, **Liu, Y. and Dong, D.** (2021). Dynamic Performance Enhancement Method Based on Improved Model Reference Adaptive System for SPMSM Sensorless Drives, *IEEE Access*, *9*, 135012–135023.

[31] **Foo, G. and Rahman, M.F.** (2010). Sensorless Sliding-Mode MTPA Control of an IPM Synchronous Motor Drive Using a Sliding-Mode Observer and HF Signal Injection, *IEEE Transactions on Industrial Electronics*, *57*(4), 1270–1278.

[32] **Yoo, J.**, **Kim, H.S. and Sul, S.K.** (2022). MTPA Tracking Control of Sensorless IPMSM Based on Square-Wave Voltage Signal Injection, *IEEE Transactions on Power Electronics*, *37*(10), 12525–12537.

[33] **Kim, W.H.**, **Lee, J.M.**, **Park, S.J. and Kim, Y.S.** (2015). Direct torque control of permanent magnet synchronous motor using a sliding-mode observer, *2015 18th International Conference on Electrical Machines and Systems (ICEMS)*, pp.1419–1422.

[34] **Guoqiang, Z.**, **Gaolin, W.**, **Ronggang, N. and Dianguo, X.** (2014). Active flux based full-order discrete-time sliding mode observer for position sensorless IPMSM drives, *2014 17th International Conference on Electrical Machines and Systems (ICEMS)*, pp.3569–3572.

[35] **Yin, Z.**, **Cao, X.**, **Zhang, Y.**, **Liu, J. and Yuan, D.** (2021). An Improved High-Order Sliding Mode Observer for IPMSM Sensorless Drive, *2021 IEEE 4th International Electrical and Energy Conference (CIEEC)*, pp.1–5.

[36] **Comanescu, M.** (2013). A sensorless sliding mode observer for the flux magnitude of the induction motor based on the synchronous reference frame model, *IECON 2013 - 39th Annual Conference of the IEEE Industrial Electronics Society*, pp.2565–2570.

[37] **Shimamoto, K. and Murakami, T.** (2022). Position and Cross-Coupling Factors Estimation for Sliding Mode Current Control Based Position-Sensorless Control of IPMSM, *IEEE Access*, *10*, 74873–74882.

[38] **Fan, Y.**, **Zhang, Q.**, **Wang, W. and Zhou, X.** (2018). Speed Regulation System of a Flux-Modulated Permanent-Magnet In-Wheel Motor Based on Sliding Mode Control and Adaptive Notch Filter, *IEEE Transactions on Energy Conversion*, *33*(4), 2183–2190.

[39] **Ye, Z. and Mohamadian, H.** (2016). Application of modern control theory on performance analysis of generalized notch filters, *2016 5th International Conference on Modern Circuits and Systems Technologies (MOCAST)*, pp.1–4.

[40] **Wu, Z.**, **Cheng, C.**, **Hua, W.**, **Wang, Y.**, **Zhang, H. and Wang, W.** (2023). A Frequency-Adaptive Delay Signal Cancelation Based Filter to Reduce Position Estimation Error for Sensorless IPMSM Drives, *IEEE Transactions on Power Electronics*, *38*(2), 1662–1671.

[41] **Chen, Y.**, **Yang, M.**, **Sun, Y.**, **Long, J.**, **Xu, D. and Blaabjerg, F.** (2021). A Modified Bi-Quad Filter Tuning Strategy for Mechanical Resonance Suppression in Industrial Servo Drive Systems, *IEEE Transactions on Power Electronics*, *36*(9), 10395–10408.

[42] **Zhang, Q.**, **Fan, Y.**, **Chen, J.**, **Yang, C. and Cheng, M.** (2022). A Current Harmonic Suppression Method for PMSM Based on Harmonic Prediction Adaptive Notch Filter, *IEEE Transactions on Energy Conversion*, *37*(3), 2107–2118.

[43] **Golnaraghi, F. and Kuo, B.C.** (2017). POLE-ZERO-CANCELLATION DESIGN: NOTCH FILTER, *Chap. 11-6 in Automatic Control Systems. 10th ed. New York: McGraw-Hill Education.*

[44] **Zheng, S.**, **Chen, Q. and Ren, H.** (2016). Active Balancing Control of AMB-Rotor Systems Using a Phase-Shift Notch Filter Connected in Parallel Mode, *IEEE Transactions on Industrial Electronics*, *63*(6), 3777–3785.

CURRICULUM VITAE

Name Surname **: Navid DELFEKAR BAGHBANI**

EDUCATION **:**

- **B.Sc.** **:** 2016, Azarbaijan Shahid Madani University, Faculty of Electrical and Electronics, Department of Electrical Engineering

PUBLICATIONS, PRESENTATIONS AND PATENTS ON THE THESIS:

- **Navid Delfekar Baghbani** Salih Barış Öztürk, 2023. ESTIMATED POSITION ERROR REDUCTION OF SMO SENSORLESS CONTROL FED IPMSM USING VARIABLE NOTCH FILTER. *INTERNATIONAL GRADUATE RESEARCH SYMPOSIUM - IGRS'23*, May 16–18, 2023 Istanbul, Turkey.

N. Delfekar Baghbani	ESTIMATED POSITION ERROR REDUCTION OF SMO-BASED SENSORLESS CONTROL OF IPMSM USING VARIABLE NOTCH FILTER	2023